

Numerical Heat Transfer, Part B: Fundamentals



An International Journal of Computation and Methodology

ISSN: 1040-7790 (Print) 1521-0626 (Online) Journal homepage: http://www.tandfonline.com/loi/unhb20

Implementation of boundary conditions in the finite-volume pressure-based method—Part I: Segregated solvers

Fadl Moukalled, Luca Mangani & Marwan Darwish

To cite this article: Fadl Moukalled, Luca Mangani & Marwan Darwish (2016) Implementation of boundary conditions in the finite-volume pressure-based method—Part I: Segregated solvers, Numerical Heat Transfer, Part B: Fundamentals, 69:6, 534-562, DOI: 10.1080/10407790.2016.1138748

To link to this article: http://dx.doi.org/10.1080/10407790.2016.1138748

	Published online: 02 May 2016.
	Submit your article to this journal 🗷
ılıl	Article views: 168
a`	View related articles 🗹
CrossMark	View Crossmark data 🗹

Full Terms & Conditions of access and use can be found at http://www.tandfonline.com/action/journalInformation?journalCode=unhb20



Implementation of boundary conditions in the finite-volume pressure-based method—Part I: Segregated solvers

Fadl Moukalled^a, Luca Mangani^b, and Marwan Darwish^a

^aDepartment of Mechanical Engineering, American University of Beirut, Beirut, Lebanon; ^bHochschule Luzern, Technik und Architektur, Horw, Switzerland

ABSTRACT

The paper deals with the formulation of a variety of boundary conditions for incompressible and compressible flows in the context of the segregated pressure-based unstructured finite volume method. The focus is on the derivation and the implementation of these boundary conditions and their relation to the various physical boundaries and geometric constraints. While a variety of boundary conditions apply at any of the physical boundaries (inlets, outlets, and walls), geometric constraints define the type of boundary condition to be used. The emphasis is on relating the mathematical derivation of the boundary conditions to the algebraic equations defined at each centroid of the boundary elements and their coefficients. All derived boundary conditions are validated through a set of test cases with comparison of computed results to available numerical and/or experimental data.

ARTICLE HISTORY

Received 8 September 2015 Accepted 24 November 2015

Introduction

The Finite Volume Method (FVM) is the most popular numerical technique in Computational Fluid Dynamics (CFD). This is not surprising since both the FVM and the velocity-pressure coupling algorithms at the core of the CFD solution algorithms, and exemplified by the SIMPLE algorithm [1, 2], originated within the same CFD group at the Imperial College [3]. Nowadays, the SIMPLE algorithm and its variants [4–13] are being successfully used to solve a wide spectrum of flow problems ranging from incompressible low speed flows [1–3, 14–18] to compressible hypersonic flows [19–24], single [25–28] and multiphase flows [29–35], laminar [25–28] and turbulent flows [36–41], free-surface flows [42, 43], and particle laden flows, to cite a few.

Furthermore, many of the issues encountered in the discretization of the conservation equations governing fluid flow and transport phenomena problems have been well documented in numerous papers [19, 22, 24] and books [2, 44]. Information on boundary conditions in general and details on their implementation in particular have not received comparable scrutiny, and except for a few papers and books [2, 44–49], they have only been reported in very general terms, this in spite of the critical role they play in ensuring the accuracy, correctness, and robustness of the numerical solutions.

It is the purpose of this article to present a detailed and comprehensive review of boundary conditions as applied to pressure based segregated finite volume solvers for the solution of incompressible and compressible flow problems. This is done using a unified and consistent notation and details down to the form of the boundary element coefficients.

To set the ground for the derivations, the discretized forms of the continuity, momentum, and energy equations governing incompressible and compressible flows are first presented. This is



	Nomenc	lature	
$a_C^{\mathbf{v}}, a_F^{\mathbf{v}}$	coefficients in discretized momentum equations	V	cell volume
a_C^{ϕ}, a_F^{ϕ} $\mathbf{b}_C^{\mathbf{v}}$ b_C^{ϕ} c_P C_{ρ}	coefficients in discretized equations source term in the discretized momentum equation source term in the discretized equations specific heat at constant pressure variable equal to $1/RT$	Greek σ_{\perp} μ γ	Symbols general variable normal stress dynamic viscosity ratio of specific heats fluid density
$egin{aligned} \mathbf{d}_{CF} \ d_{CF} \ \mathbf{D} \end{aligned}$	vector joining the grid points C and F magnitude of \mathbf{d}_{CF} tensor operator	τ Ψ, Φ	deviatoric stress tensor dissipation terms in energy equation
\mathcal{D} e E E f_b f_b f	scalar defined by Eq. (17) unit vector Distance vector in the direction of \mathbf{d}_{CF} magnitude of \mathbf{E} body force per unit volume force exerted by wall on fluid identity matrix thermal conductivity chord length Mach number mass flow rate pressure pressure pressure correction best generation per unit volume	Subscript	refers to boundary refers to main grid point refers to control volume face refers to the F grid point refers to values at the faces obtained by interpolation between C and its neighbors refers to the neighbors of the C grid point refers to wall refer to x,y, and z component, respectively refers to stagnation condition component of a vector parallel to a surface component of a vector normal to a surface
qv R S S t T T u, v, w	heat generation per unit volume gas constant surface vector magnitude of S time temperature vector equal to $S - E$ velocity components in x , y , and z direction, respectively velocity vector	Superso p T T u, v, w n … *	refers to pressure refers to temperature refers to the transpose of a vector refers to the u, v, and w-velocity component, respectively refers to value at the previous iteration refers to an interpolated value refers to an updated value during an iteration refers to an old time value

followed by a thorough review of frequently used boundary conditions with complete details on the related discretization and implementation issues. Finally, a set of test problems involving many of the cited boundary conditions are used as validation tests.

The governing equations

The mass, momentum, and energy equations governing fluid flow and heat transfer problems are written as

$$\frac{\partial \rho}{\partial t} + \nabla \cdot (\rho \mathbf{v}) = 0, \tag{1}$$

$$\frac{\partial}{\partial t}[\rho \mathbf{v}] + \nabla \cdot {\{\rho \mathbf{v} \mathbf{v}\}} = -\nabla p + [\nabla \cdot \mathbf{\tau}] + \mathbf{f}_{b}, \tag{2}$$

$$\frac{\partial}{\partial t} (\rho c_p T) + \nabla \cdot \left[\rho c_p \mathbf{v} T \right] = \nabla \cdot \left[k \nabla T \right] + \rho T \frac{D c_p}{D t} + \frac{D p}{D t} - \frac{2}{3} \mu \Psi + \mu \Phi + \dot{q}_V, \tag{3}$$

where \mathbf{v} , p, T, ρ , \mathbf{f}_{b} , c_{p} , k, μ , and \dot{q}_{V} represent the velocity vector, pressure, temperature, density, body force per unit volume, specific heat at constant pressure, thermal conductivity, dynamic viscosity, and heat generation per unit volume, respectively. In addition, τ is the deviatoric stress tensor, which, for a Newtonian fluid is given by

$$\tau = \mu \left\{ \nabla \mathbf{v} + (\nabla \mathbf{v})^{\mathrm{T}} \right\} - \frac{2}{3} \mu (\nabla \cdot \mathbf{v}) \mathbf{I}. \tag{4}$$

For compressible flow, an equation of state relating density to temperature and pressure is required. For an ideal gas this equation is written as

$$\rho = \frac{p}{RT},\tag{5}$$

where R is the gas constant.

The discretized equations

In the FVM the discretization process starts by integrating the governing equations over the cells into which the domain has been subdivided (Figure 1) and with the divergence theorem, the volume integrals of the convection and diffusion terms are transformed into surface integrals. The resulting surface integrals and the volume integrals of the transient and other source terms are expressed in terms of the discrete volumes of the respective elements. In a second step, numerical integration is performed producing a set of semi-discretized equations that represent surface and volume fluxes. Finally, linearizing these fluxes and expressing them in terms of the unknowns defined at element centroids yields a set of algebraic equations that represents the numerical equivalent of the original conservation equations. Details on this procedure can be found in the literature [2, 19, 22, 24, 44]. In this work, this represents the starting point of the derivations. A summary of these equations is presented next with their forms obtained using an upwind scheme for the discretization of the convection term and an implicit backward Euler scheme for the transient term.

The discretized momentum equation

Designating the value of the dependent variable at the centroid of an element and at an element face with subscript C and f, respectively, the discretized momentum equation using vector

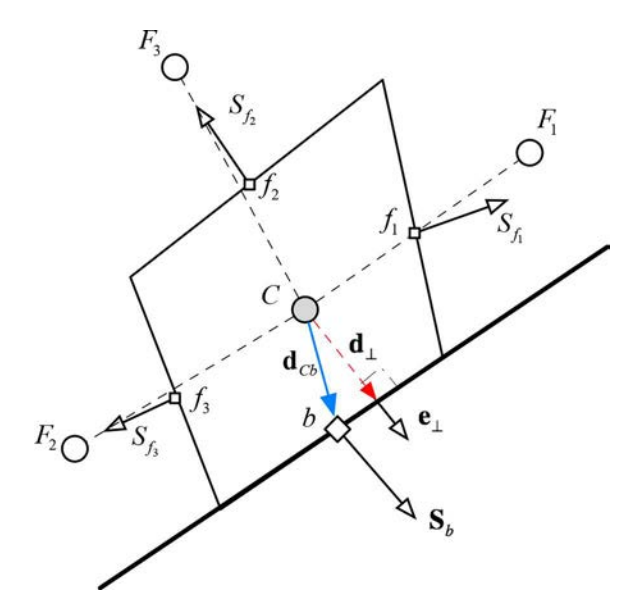


Figure 1. An example of a boundary element.

$$a_{\mathbf{C}}^{\mathbf{v}}\mathbf{v}_{\mathbf{C}} + \sum_{\mathbf{F} = NB(\mathbf{C})} a_{\mathbf{F}}^{\mathbf{v}}\mathbf{v}_{\mathbf{F}} = \mathbf{b}_{\mathbf{C}}^{\mathbf{v}}$$

$$\tag{6}$$

with the coefficients calculated using the following expressions:

$$a_{\mathrm{C}}^{\mathbf{v}} = \frac{\rho_{\mathrm{C}} V_{\mathrm{C}}}{\Delta t} + \sum_{f=nb(C)} \|\dot{m}_{\mathrm{f}}, 0\| + \sum_{f=nb(C)} \mu_{\mathrm{f}} \frac{E_{\mathrm{f}}}{d_{\mathrm{CF}}}$$

$$a_{\mathrm{F}}^{\mathbf{v}} = -\|-\dot{m}_{\mathrm{f}}, 0\| - \mu_{\mathrm{f}} \frac{E_{\mathrm{f}}}{d_{\mathrm{CF}}}$$

$$\mathbf{b}_{\mathrm{C}}^{\mathbf{v}} = \frac{\rho_{\mathrm{C}}^{\circ} V_{\mathrm{C}}}{\Delta t} \mathbf{v}_{\mathrm{C}}^{\circ} + (\mathbf{f}_{\mathrm{b}})_{\mathrm{C}} V_{\mathrm{C}} + \sum_{f=nb(C)} \left(\mu_{\mathrm{f}}(\nabla \mathbf{v})_{\mathrm{f}} \cdot \mathbf{T}_{\mathrm{f}}\right) + \sum_{f=nb(C)} \mu_{\mathrm{f}}(\nabla \mathbf{v})_{\mathrm{f}}^{\mathrm{T}} \cdot \mathbf{S}_{\mathrm{f}} - (\nabla p)_{\mathrm{C}} V_{\mathrm{C}} - \underbrace{(2/3) \sum_{f=nb(C)} (\mu \nabla \cdot \mathbf{v})_{\mathrm{f}} \mathbf{S}_{\mathrm{f}}}_{\text{compressible contribution}}$$

$$(7)$$

The mass flow rate at a cell face is defined as

$$\dot{m}_{\rm f} = \rho_{\rm f} \mathbf{v}_{\rm f} \cdot \mathbf{S}_{\rm f} \tag{8}$$

with the interface velocity calculated using the Rhie-Chow interpolation technique [38] as

$$\mathbf{v}_{\mathrm{f}} = \overline{\mathbf{v}_{\mathrm{f}}} - \overline{\mathbf{D}_{\mathrm{f}}^{\mathbf{v}}} (\nabla p_{\mathrm{f}} - \overline{\nabla p_{\mathrm{f}}}) \tag{9}$$

In Eq. (9), the bar indicates a value obtained by interpolation. Moreover, $\overline{D_f^v}$ can be written simply as

$$\overline{\mathbf{D}_{\mathrm{f}}^{\mathbf{v}}} = \overline{\left(\frac{V_{\mathrm{C}}}{a_{\epsilon}^{\mathbf{v}}}\right)} \tag{10}$$

Also, S_f is the surface vector, d_{CF} is the magnitude of the vector \mathbf{d}_{CF} joining C and F, and E_f is the magnitude of the vector \mathbf{E}_{f} , which is related to \mathbf{S}_{f} and \mathbf{T}_{f} via the following equation:

$$\mathbf{S}_{\mathbf{f}} = \mathbf{E}_{\mathbf{f}} + \mathbf{T}_{\mathbf{f}} \tag{11}$$

where $\mathbf{E}_{\rm f}$ is set in the direction of $\mathbf{d}_{\rm cf}$ [47, 50–52].

The discretized continuity equation

In the segregated pressure-based SIMPLE algorithm adopted here, the continuity equation is not solved directly. Rather, a pressure correction variable (p') is defined and the semi-discretized form of the continuity equation is transformed into a pressure correction equation by combining it with the algebraic form of the momentum equation [19, 22, 24]. The final algebraic form of this equation is written as

$$a_{\rm C}^{p'}p_{\rm C}' + \sum_{F=NB(C)} a_{\rm F}^{p'}p_{\rm F}' = b_{\rm C}^{p'} \tag{12}$$

with its coefficients given by

$$a_{\mathrm{F}}^{p'} = -\rho_{\mathrm{f}}^{*} \mathcal{D}_{\mathrm{f}} - \underbrace{\left\| -\dot{m}_{\mathrm{f}}^{*}, 0 \right\| \frac{C_{\rho, \mathrm{f}}}{\rho_{\mathrm{f}}^{*}}}_{\text{compressible contribution}}$$

$$a_{\mathrm{C}}^{p'} = \underbrace{\frac{V_{\mathrm{C}} C_{\rho, \mathrm{C}}}{\Delta t} + \sum_{f = nb(C)} \left(\frac{C_{\rho, \mathrm{f}}}{\rho_{\mathrm{f}}^{*}} \left\| \dot{m}_{\mathrm{f}}^{*}, 0 \right\| \right)}_{\text{compressible contribution}} + \sum_{f = nb(C)} \rho_{\mathrm{f}}^{*} \mathcal{D}_{\mathrm{f}}$$

$$b_{\mathrm{C}}^{p'} = -\left(\underbrace{\frac{\left(\rho_{\mathrm{C}}^{*} - \rho_{\mathrm{C}}^{\circ}\right)}{\Delta t} V_{\mathrm{C}}}_{\text{compressible contribution}} + \sum_{f = nb(C)} \dot{m}_{\mathrm{f}}^{*} \right)$$

$$(13)$$

where superscript * refers to values obtained from solving the momentum equation during the same iteration and superscript $^{\circ}$ refers to old values, i.e., values from the previous time step. For an ideal gas the term C_{ρ} is computed as

$$C_{\mathsf{p}} = \frac{1}{RT} \tag{14}$$

Moreover, by neglecting the non-orthogonal contribution of $\left(\mathbf{D}_{f}^{v}\nabla p'_{f}\right)\cdot\mathbf{S}_{f}$, \mathcal{D}_{f} is calculated such that

$$\left(\mathbf{D}_{f}^{\mathbf{v}}\nabla p_{f}'\right) \cdot \mathbf{E}_{f} = \mathcal{D}_{f}\left(p_{F}' - p_{C}'\right) \tag{15}$$

The discretized energy equation

The discretization of the energy equation leads to the following algebraic relation:

$$a_{\mathcal{C}}^T T_{\mathcal{C}} + \sum_{F = NB(\mathcal{C})} a_{\mathcal{F}}^T T_{\mathcal{F}} = b_{\mathcal{C}}^T \tag{16}$$

with the expressions for the coefficients given by

$$a_{\rm F}^{T} = -k_{\rm f} \frac{E_{\rm f}}{d_{\rm CF}} - \|-\dot{m}_{\rm f}, 0\| (c_{\rm p})_{\rm f}$$

$$a_{\rm C}^{T} = a_{\rm C}^{-} \sum_{F=NB(C)} a_{\rm F}^{T} + \sum_{f=nb(C)} \dot{m}_{\rm f} (c_{\rm p})_{\rm f} + \|-a_{\rm C}^{c_{\rm p}}, 0\|$$

$$a_{\rm C}^{=} \frac{\rho_{\rm C}(c_{\rm p})_{\rm C} V_{\rm C}}{\Delta t} \qquad a_{\rm C}^{\circ} = \frac{\rho_{\rm C}^{\circ}(c_{\rm p}^{\circ})_{\rm C} V_{\rm C}}{\Delta t} \qquad a_{\rm C}^{c_{\rm p}} = \rho_{\rm C} V_{\rm C} \left(\frac{Dc_{\rm p}}{Dt}\right)_{\rm C}$$

$$b_{\rm C}^{T} = \sum_{f=nb(C)} \left(k_{\rm f}(\nabla T)_{\rm f} \cdot \mathbf{T}_{\rm f}\right) + a_{\rm C}^{\circ} T_{\rm C}^{\circ} + T_{\rm C} \|a_{\rm C}^{c_{\rm p}}, 0\| + \left[\left(\frac{Dp}{Dt}\right)_{\rm C} + \mu_{\rm C}\left(-\frac{2}{3}\Psi_{\rm C} + \Phi_{\rm C}\right) + (\dot{q}_{\rm V})_{\rm C}\right] V_{\rm C}$$

$$(17)$$

where k is the fluid thermal conductivity, and (D/Dt) is the material derivative.



Boundary conditions

It is important to differentiate between physical conditions, geometric constraints, and boundary conditions at a domain boundary. An "Inlet", an "Outlet", or a "Wall" represents a physical condition, while "Symmetry" and "Periodicity" represent geometric constraints. A boundary condition refers to the set of equations used along a domain boundary to obtain a specific solution to the problem. For a given physical condition, the boundary condition depends on the equation solved and its known variables, with several options possible. For example on a physical "Wall", the boundary condition for the momentum equation could be a slip or a no-slip condition, while for the energy equation it could be a specified flux, an imposed temperature, or a convection heat transfer condition. A variety of boundary conditions will also apply to other physical conditions; at an "Inlet", it is possible to enforce a specified pressure and velocity direction, or to describe the velocity components without assigning any value for the pressure. On the other hand, one boundary condition describes a geometric condition, usually imposed with the intention of reducing the size of the computational domain. For example, the only boundary condition applicable along a symmetry line is a zero normal flux.

Generally, the boundary conditions used are a part of one of the following three basic categories:

- 1. a Dirichlet condition, where the unknown variable is defined at the boundary;
- 2. a von Neumann condition, where the flux expressed in the conservation equation is defined at the boundary face;
- 3. a Robin-type condition, where the unknown variable and flux at the boundary are expressed via a constitutive relation.

Boundary conditions apply to boundary elements, which are elements that have at least one boundary face (Figure 1).

For the pressure correction equation, which plays a central role in solving flow problems via the Navier–Stokes equations, these categories are expressed as follows:

- 1. a von Neumann like boundary condition whereby \dot{m}_b is specified (e.g., walls) with no need to modify the p' equation. The boundary pressure however is extrapolated from the interior field;
- 2. a Dirichlet-like boundary condition whereby a boundary pressure p_b is defined. In this case \dot{m}_b is written in terms of the nearest element velocity vector and pressure gradient;
- 3. a Robin-type boundary condition specified via an implicit relation between pressure and velocity from which an explicit formula is derived and substituted in the pressure correction equation.

Another important issue to consider is related to the way by which the Rhie-Chow interpolation at a boundary face is handled. Specifically the averaging procedure is modified at boundary faces so that the boundary face average is written in terms of the element value as

$$\overline{\square}_{b} = \square_{C} \tag{18}$$

where b and C refer to the boundary face and the element centroid, respectively, and to any variable or expression. Adopting this practice transforms the velocity at a boundary face from the expression given by Eq. (9) into

$$\mathbf{v}_{b}^{*} = \mathbf{v}_{C}^{*} - \mathbf{D}_{C}^{\mathbf{v}} \left(\nabla p_{b}^{(n)} - \nabla p_{C}^{(n)} \right) \tag{19}$$

Discretized boundary equations

In the derivation of boundary conditions, it is sometimes more insightful to use the conservation equations in their semi-discretized form rather than their algebraic form. To this end, the semi-discretized forms of the momentum, continuity, and energy equations for a boundary element with a boundary face are expressed as

$$\frac{(\rho \mathbf{v})_{\mathbf{C}} - (\rho \mathbf{v})_{\mathbf{C}}^{\circ}}{\Delta t} V_{\mathbf{C}} + \sum_{f = \text{interior } nb(\mathbf{C})} (\dot{m}_{\mathbf{f}} \mathbf{v}_{\mathbf{f}}) + \dot{m}_{\mathbf{b}} \mathbf{v}_{\mathbf{b}} = - \underbrace{p_{\mathbf{b}} \mathbf{S}_{\mathbf{b}}}_{\text{boundary face}} + \underbrace{t_{\mathbf{b}} \cdot \mathbf{S}_{\mathbf{b}}}_{\text{boundary face}} - \sum_{\text{boundary face}} (p_{\mathbf{f}} \mathbf{S}_{\mathbf{f}}) + \sum_{f = \text{interior } nb(\mathbf{C})} (\tau_{\mathbf{f}} \cdot \mathbf{S}_{\mathbf{f}}) + \mathbf{B}_{\mathbf{C}}$$

$$\frac{(\rho_{\mathbf{C}}^{*} - \rho_{\mathbf{C}}^{\circ})}{\Delta t} V_{\mathbf{C}} + \sum_{f = \text{interior } nb(\mathbf{C})} \dot{m}_{\mathbf{f}} + \dot{m}_{\mathbf{b}} = \underbrace{(p_{\mathbf{C}}^{*} - \rho_{\mathbf{C}}^{\circ})}_{\text{boundary face}} V_{\mathbf{C}} + \underbrace{\sum_{f = \text{interior } nb(\mathbf{C})} (\dot{m}_{\mathbf{f}}^{*} + \dot{m}_{\mathbf{f}}^{*}) + \underbrace{(\dot{m}_{\mathbf{b}}^{*} + \dot{m}_{\mathbf{b}}^{*})}_{\text{boundary face}} = 0$$

$$\frac{(\rho c_{\mathbf{p}} T)_{\mathbf{C}} - (\rho c_{\mathbf{p}} T)_{\mathbf{C}}^{\circ}}{\Delta t} V_{\mathbf{C}} + \sum_{f = \text{interior } nb(\mathbf{C})} (\dot{m} c_{\mathbf{p}} T)_{\mathbf{f}} + \underbrace{(\dot{m} c_{\mathbf{p}} T)_{\mathbf{b}}}_{\text{boundary face}} = 0$$

$$\frac{(\rho c_{\mathbf{p}} T)_{\mathbf{C}} - (\rho c_{\mathbf{p}} T)_{\mathbf{C}}^{\circ}}{\Delta t} V_{\mathbf{C}} + \sum_{f = \text{interior } nb(\mathbf{C})} (\dot{m} c_{\mathbf{p}} T)_{\mathbf{f}} + \underbrace{(\dot{m} c_{\mathbf{p}} T)_{\mathbf{b}}}_{\text{boundary face}} = 0$$

$$\frac{(\rho c_{\mathbf{p}} T)_{\mathbf{C}} - (\rho c_{\mathbf{p}} T)_{\mathbf{C}}^{\circ}}{\Delta t} V_{\mathbf{C}} + \sum_{f = \text{interior } nb(\mathbf{C})} (\dot{m} c_{\mathbf{p}} T)_{\mathbf{f}} + \underbrace{(\dot{m} c_{\mathbf{p}} T)_{\mathbf{b}}}_{\text{boundary face}} = 0$$

$$\frac{(\rho c_{\mathbf{p}} T)_{\mathbf{C}} - (\rho c_{\mathbf{p}} T)_{\mathbf{C}}^{\circ}}{\Delta t} V_{\mathbf{C}} + \sum_{f = \text{interior } nb(\mathbf{C})} (\dot{m} c_{\mathbf{p}} T)_{\mathbf{f}} + \underbrace{(\dot{m} c_{\mathbf{p}} T)_{\mathbf{b}}}_{\text{boundary face}} = 0$$

$$\frac{(\rho c_{\mathbf{p}} T)_{\mathbf{C}} - (\rho c_{\mathbf{p}} T)_{\mathbf{C}}^{\circ}}{\Delta t} V_{\mathbf{C}} + \sum_{f = \text{interior } nb(\mathbf{C})} (\dot{m} c_{\mathbf{p}} T)_{\mathbf{f}} + \underbrace{(\dot{m} c_{\mathbf{p}} T)_{\mathbf{b}}}_{\text{boundary face}} = 0$$

$$\frac{(\rho c_{\mathbf{p}} T)_{\mathbf{C}} - (\rho c_{\mathbf{p}} T)_{\mathbf{C}}^{\circ}}{\Delta t} V_{\mathbf{C}} + \sum_{f = \text{interior } nb(\mathbf{C})} (\dot{m} c_{\mathbf{p}} T)_{\mathbf{C}} + \underbrace{(\dot{m} c_{\mathbf{p}} T)_{\mathbf{c}}}_{\text{boundary face}} = 0$$

$$\frac{(\rho c_{\mathbf{p}} T)_{\mathbf{C}} - (\rho c_{\mathbf{p}} T)_{\mathbf{C}}^{\circ}}{\Delta t} V_{\mathbf{C}} + \sum_{f = \text{interior } nb(\mathbf{C})} (\dot{m} c_{\mathbf{p}} T)_{\mathbf{C}} + \underbrace{(\dot{m} c_{\mathbf{p}} T)_{\mathbf{C}}}_{\mathbf{C}} + \underbrace{(\dot{m} c_{\mathbf{p}} T)_{\mathbf{C}}}_{\mathbf{C}} + \underbrace{(\dot{m} c_{\mathbf{p}} T)_{\mathbf{C}}}_{\mathbf{C}} + \underbrace{(\dot{m} c_{\mathbf{p}} T)_{\mathbf{C}}}_{\mathbf{C}} + \underbrace{(\dot{m} c_{\mathbf{p}} T)_{\mathbf{$$

where f refers to an interior face, b to a boundary face, superscript * to a value obtained after solving the momentum equation, and prime to a correction term. Terms evaluated at the boundary face are written explicitly as they should be modified based on the type of boundary condition used. With an average quantity at the boundary written in terms of the boundary cell value, combining Eq. (18) with Eqs. (15) and (19) results in the following equations for the boundary mass flow rate and its correction:

$$\dot{m}_{b} = \rho_{b}^{*} \mathbf{v}_{C}^{*} \cdot \mathbf{S}_{b} - \rho_{b}^{*} \mathbf{D}_{C}^{\mathbf{v}} \left(\nabla p_{b}^{(n)} - \nabla p_{C}^{(n)} \right) \cdot \mathbf{S}_{b} + \underbrace{\left(\frac{\dot{m}_{b}^{*}}{\rho_{b}^{*}} \right) \rho_{b} - \dot{m}_{b}^{*}}_{\text{compressible}}$$

$$\dot{m}'_{b} = -\rho_{b}^{*} \mathcal{D}_{C} \left(p'_{b} - p'_{C} \right) + \underbrace{\left(\frac{\dot{m}_{b}^{*}}{\rho_{b}^{*}} \right) C_{\rho, b} p'_{b}}_{\text{compressible contribution}}$$
(23)

With these definitions the boundary conditions for incompressible and then compressible flows can now be presented for the various physical and geometric conditions. For completeness all derivations will start with Eqs. (20)–(23).

Incompressible flow

The most common types of boundary conditions encountered in solving incompressible flow problems are presented next.

Physical condition: Wall

At a stationary or a moving wall, a no-slip (Figure 2a) or a slip (Figure 2b) boundary condition is usually applied. The following paragraphs describe the implementation of both conditions.

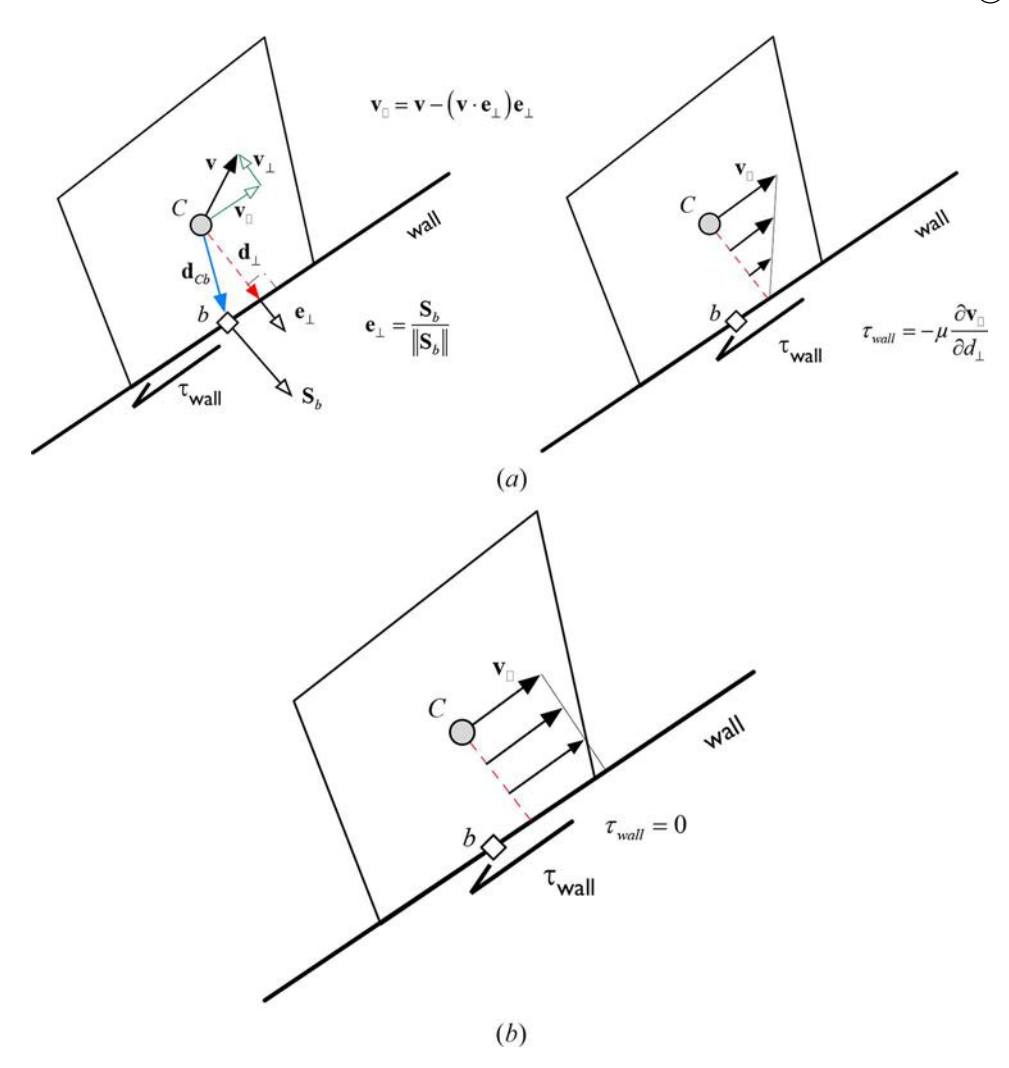


Figure 2. (a) Schematics of a no-slip wall boundary condition, (b) schematic of a slip wall boundary condition.

Boundary condition: No-slip wall

This boundary condition is used for viscous flows and indicates that the fluid velocity \mathbf{v}_b is equal to the wall velocity \mathbf{v}_{wall} (zero for a stationary wall). The pressure at the wall is set to ensure a stagnation point for the velocity component normal to the wall, while the velocity component parallel to the wall defines the value of the wall shear stress. This is akin to a shear flux applied to the component of the momentum equation parallel to the wall and to a Dirichlet condition applied to the normal component. For the pressure correction equation, this is similar to a von Neumann condition applied to the boundary face.

Momentum equation

A common misconception in the application of the no slip condition is to view it as a Dirichlet boundary condition. While this treatment leads to correct results for Cartesian grids, it does not do so for general curvilinear grids. As shown in Figure 2a, a correct implementation of this boundary condition should guarantee that the shear stress τ_{wall} (and consequently the force F_b) is tangent to the

 $\underbrace{a_{\text{C}}}_{\textit{interior faces contribution}}$ $\begin{array}{c} + \\ \frac{\mu_{b}S_{b}}{d_{\perp}} \left(1 - e_{\perp x}^{2}\right) \\ \frac{\mu_{b}S_{b}}{d_{\perp}} \left(1 - e_{\perp y}^{2}\right) \\ \frac{\mu_{b}S_{b}}{d_{\perp}} \left(1 - e_{\perp z}^{2}\right) \\ 0 \\ k_{b} \frac{E_{b}}{d_{cb}} \\ 0 \\ \frac{h_{\infty}S_{b}k_{b} \frac{E_{b}}{d_{cb}}}{h_{\infty}S_{b} + k_{b} \frac{E_{b}}{d_{cb}}} \end{array}$ $\frac{\mu_{b}S_{b}}{d_{\perp}}\left[u_{b}\left(1-e_{\perp x}^{2}\right)+\left(v_{C}-v_{b}\right)e_{\perp y}e_{\perp x}+\left(w_{C}-w_{b}\right)e_{\perp z}e_{\perp x}\right]-\rho_{b}S_{b}^{x}$ $\frac{\mu_{b}S_{b}}{d_{\perp}}\left[\left(u_{C}-u_{b}\right)e_{\perp x}e_{\perp y}+v_{b}\left(1-e_{\perp y}^{2}\right)+\left(w_{C}-w_{b}\right)e_{\perp z}e_{\perp y}\right]-\rho_{b}S_{b}^{y}$ $\frac{\mu_{b}S_{b}}{d_{\perp}}\left[\left(u_{C}-u_{b}\right)e_{\perp x}e_{\perp z}+\left(v_{C}-v_{b}\right)e_{\perp y}e_{\perp z}+w_{b}\left(1-e_{\perp z}^{2}\right)\right]-\rho_{b}S_{b}^{y}$ 02 4 $\begin{aligned} & k_{b} \frac{\underline{f_{b}}}{d_{cb}} T_{\text{specified}} + \left(k \nabla T\right)_{b} \cdot \mathbf{T}_{b} \\ & - q_{\text{specified}} S_{b} \\ & \underline{h_{\infty}} S_{b} k_{b} \\ & \underline{h_{\infty}} S_{b} + k_{b} \frac{\underline{f_{b}}}{d_{cb}} \left(\frac{\underline{F_{b}}}{d_{cb}} T_{\infty} + \left(\nabla T\right)_{b} \cdot \mathbf{T}_{b}\right) \end{aligned}$ 6 0 0

Modified coefficients of the momentum, continuity, and energy equations for a no-slip wall boundary condition.

wall along with $\mathbf{v}_b = \mathbf{v}_{wall}$. The force \mathbf{F}_b can be written as

$$\mathbf{F}_{b} = \tau_{\text{wall}} S_{b} = -\mu \frac{\partial \mathbf{v}_{\parallel}}{\partial d_{\perp}} S_{b} \tag{24}$$

where \mathbf{v}_{\parallel} is the component of velocity parallel to the wall and d_{\perp} the normal distance to the wall, both given by

$$\mathbf{v}_{\parallel} = \mathbf{v} - \underbrace{\mathbf{v}_{\perp}}_{\text{pormal component}} \quad \mathbf{v}_{\perp} = (\mathbf{v} \cdot \mathbf{e}_{\perp}) \mathbf{e}_{\perp} \quad d_{\perp} = \mathbf{d}_{Cb} \cdot \mathbf{e}_{\perp} = \mathbf{d}_{Cb} \cdot \frac{\mathbf{S}_{b}}{S_{b}}$$
 (25)

An approximation for the wall shear stress can be derived from Eq. (24) and is written as

$$\tau_{\text{wall}} \approx -\mu_{\text{b}} \frac{(\mathbf{v}_{\text{C}} - \mathbf{v}_{\text{b}})_{\parallel}}{d_{\perp}} = -\mu_{\text{b}} \frac{(\mathbf{v}_{\text{C}} - \mathbf{v}_{\text{b}}) - [(\mathbf{v}_{\text{C}} - \mathbf{v}_{\text{b}}) \cdot \mathbf{e}_{\perp}] \mathbf{e}_{\perp}}{d_{\perp}}$$
(26)

Combining Eqs. (26) and (24), the modified coefficients for the boundary elements of the x, y, and z components of the momentum equation are obtained with their expressions displayed in Table 1a (rows 1-3).

Continuity or pressure correction equation

Since at a wall the mass flow rate is zero, the mass flow rate correction is also zero ($\dot{m}'_b = 0$), with no modifications required for the pressure-correction equation. The pressure p_b at the boundary is obtained by extrapolation as

$$p_{\rm b} = p_{\rm C} + \nabla p_{\rm C}^{(n)} \cdot \mathbf{d}_{\rm Cb} \tag{27}$$

The coefficient of the boundary element is modified as displayed in row 4 of Table 1a.

Energy equation

Since at the wall \dot{m}_b is zero, the term $(\dot{m}c_pT)_b$ is zero. The only modification is for the diffusion flux, which can be specified in three different ways such as using the wall temperature (Dirichlet boundary condition), the wall heat flux (von Neumann boundary condition), or by defining a heat transfer coefficient and a surrounding temperature (mixed or Robin-type boundary condition). Details of these three types are as follows.

Dirichlet boundary condition

For this type the temperature is specified at the boundary, i.e.

$$T_{\rm b} = T_{\rm specified}$$
 (28)

The diffusion flux at the wall is computed as

$$(k\nabla T \cdot \mathbf{S})_{b} = (k\nabla T)_{b} \cdot (\mathbf{E}_{b} + \mathbf{T}_{b}) = k_{b} \frac{E_{b}}{d_{Cb}} (T_{b} - T_{C}) + (k\nabla T)_{b} \cdot \mathbf{T}_{b}$$
(29)

leading to the modified coefficients of the boundary element shown in row 5 of Table 1a.

Von Neumann boundary condition

For this type, the boundary flux is known, i.e.

$$q_{b}S_{b} = q_{\text{specified}}S_{b} = -(k\nabla T \cdot \mathbf{S})_{b}$$
(30)

The modifications to the coefficients of the boundary element are shown in row 6 of Table 1a.

Mixed (or Robin-type) boundary condition

For this boundary condition a convection heat transfer coefficient (h_{∞}) and a surrounding temperature (T_{∞}) are specified. At the wall, the diffusion flux is set equal to the convection flux to give

$$(k\nabla T \cdot \mathbf{S})_{b} = k_{b} \frac{E_{b}}{d_{Cb}} (T_{b} - T_{C}) + (k\nabla T)_{b} \cdot \mathbf{T}_{b}$$
$$= h_{\infty} (T_{\infty} - T_{b}) S_{b}$$
(31)

Using Eq. (31), the wall temperature (T_b) is expressed as

$$T_{\rm b} = \frac{h_{\infty} S_{\rm b} T_{\infty} + k_{\rm b} \frac{E_{\rm b}}{d_{\rm Cb}} T_{\rm C} - (k \nabla T)_{\rm b} \cdot \mathbf{T}_{\rm b}}{h_{\infty} S_{\rm b} + k_{\rm b} \frac{E_{\rm b}}{d_{\rm cc}}}$$
(32)

Substitution of Eq. (32) in Eq. (31), yields the boundary flux as

$$(k\nabla T \cdot \mathbf{S})_{b} = \frac{h_{\infty}S_{b}k_{b}\frac{E_{b}}{d_{Cb}}}{h_{\infty}S_{b} + k_{b}\frac{E_{b}}{d_{Cb}}}(T_{\infty} - T_{C}) + \frac{h_{\infty}S_{b}(k\nabla T)_{b} \cdot \mathbf{T}_{b}}{h_{\infty}S_{b} + k_{b}\frac{E_{b}}{d_{Cb}}}$$
(33)

Then the coefficients of the boundary element are modified as displayed in row 7 of Table 1a.

Boundary condition: Slip wall boundary for inviscid flow

For a slip wall boundary condition the normal velocity component at the wall remains zero. However, with the shear stress set to zero, the parallel component at the wall is set equal to the parallel component of the boundary element.

Momentum equation

In this case, the shear stress at the wall is zero leading to a zero boundary force (Figure 2b). Thus, dropping the stress term from the momentum equation its coefficients become

$$a_{\rm C}^{\rm v} = \underbrace{a_{\rm C}^{\rm v}}_{\text{interior faces contribution}}$$

$$a_{F=b}^{\rm v} = 0$$

$$\mathbf{b}_{\rm C}^{\rm v} = \underbrace{\mathbf{b}_{\rm C}^{\rm v}}_{\text{interior faces contribution}} -p_{\rm b}\mathbf{S}_{\rm b}$$

$$(34)$$

Pressure correction and energy equations

The modifications to the continuity and energy equations are exactly the ones presented for the noslip case with the boundary pressure computed using Eq. (27).

Physical condition: Inlet

At the inlet to a domain, a number of boundary conditions can be imposed (Figure 3) and the ones considered here include: (i) specified velocity (Figure 3a); (ii) specified static pressure and velocity direction (Figure 3b); and (iii) specified total pressure and velocity direction (Figure 3c). For the energy equation, the temperature is usually specified.

Boundary condition: Specified velocity

Momentum equation

For an incompressible flow, a specified velocity at the inlet (Figure 3a) implies a known mass flux. Therefore, the boundary force $(\mathbf{F}_b = \mathbf{\tau}_b \cdot \mathbf{S}_b)$ and convection flux $(\dot{m}_b \mathbf{v}_b)$ are calculated using the known \dot{m}_b and \mathbf{v}_b . Similar to the no-slip boundary condition, the pressure at the boundary is extrapolated using Eq. (27). The known terms in the equation are evaluated explicitly and added to the source term with the modified boundary element coefficients given by

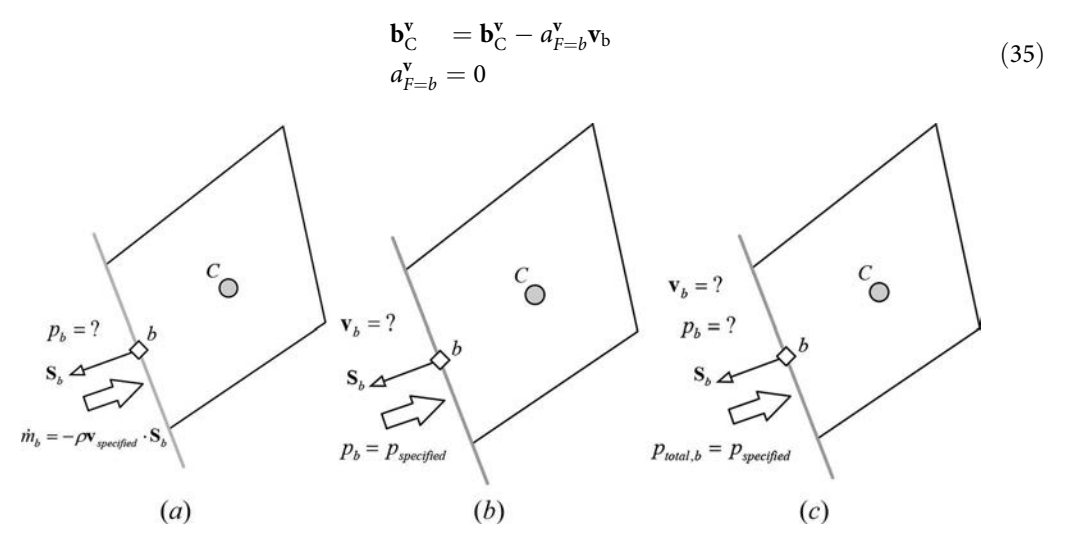


Figure 3. Schematics of (a) specified velocity (b) specified pressure and velocity direction, and (c) specified total pressure and velocity direction boundary conditions at the inlet.



Pressure correction equation

Since \dot{m}_b is known, its correction is zero, i.e., $\dot{m}_b' = 0$. Therefore, for a boundary element \dot{m}_b' is dropped with no modifications required for the coefficients (i.e., $a_{F=h}^{\mathbf{v}} = 0$).

Energy equation

For a specified static temperature at inlet, since \dot{m}_b and \mathbf{v}_b are known, the boundary terms $(\dot{m}c_pT)_b$ and $(k \nabla T \cdot S)_b$ are directly computed. As for the momentum equation, known terms in the equation for the boundary cell are evaluated explicitly and added to the source term with the modified boundary element coefficients given by

$$b_{C}^{T} = b_{C}^{T} - a_{F=b}^{T} T_{b}$$

$$a_{F=b}^{T} = 0$$
(36)

Boundary condition: Specified pressure and velocity direction

Momentum equation

For the boundary element, the known value of the inlet pressure p_b is used in the calculation of ∇p_C , which, in turn, is used in computing the velocity v_b . To be able to perform this task, the flow direction should be known (Figure 3b). Denoting the unit velocity vector by \mathbf{e}_{v} and assuming the mass flow rate has been calculated from the continuity equation as $\dot{m}_b = \dot{m}_b^* + m_b'$, \mathbf{v}_b is computed as

$$\dot{m}_{b} = \rho_{b} \|\mathbf{v}_{b}\| \mathbf{e}_{\mathbf{v}} \cdot \mathbf{S}_{b} \Rightarrow \|\mathbf{v}_{b}\| = \frac{\dot{m}_{b}}{\rho_{b}(\mathbf{e}_{\mathbf{v}} \cdot \mathbf{S}_{b})} \Rightarrow \mathbf{v}_{b} = \|\mathbf{v}_{b}\| \mathbf{e}_{\mathbf{v}}. \tag{37}$$

Thus for the momentum equation, the boundary condition is a specified velocity that is iteratively updated from the continuity equation and the equation of the boundary cell is modified according to Eq. (35).

Pressure correction equation

Since p_b is known, p'_b is zero ($\dot{m}'_b \neq 0$) and a Dirichlet boundary condition is applied. Thus, the coefficient of the boundary cell of the p' equation is modified as

$$a_{\rm C}^{p'} = \sum_{f = \text{interior } nb(C)} \rho_{\rm f} \mathcal{D}_{\rm f} + \underbrace{\rho_{\rm b} \mathcal{D}_{\rm C}}_{\text{boundary face contribution}}$$
(38)

Energy equation

For the energy equation, the temperature is usually specified. Therefore, the modifications to the coefficients of the boundary elements are similar to those given in Eq. (36).

Boundary condition: Specified total pressure and velocity direction

Momentum equation

The relation between total (p_0) and static (p) pressure for incompressible flow is given by

$$\underbrace{p_0}_{\text{total pressure}} = \underbrace{p}_{\text{static pressure}} + \underbrace{\frac{1}{2}\rho\mathbf{v}\cdot\mathbf{v}}_{\text{dynamic pressure}} .$$
(39)

The calculation of \dot{m}_b (Figure 3c) requires a special procedure, which will be explained in connection with the continuity equation. Assuming \dot{m}_b is known, \mathbf{v}_b is calculated using Eq. (37) and the coefficients in the momentum equation are modified according to Eq. (35).

Pressure correction equation

Since p_b is unknown, p'_b is not zero and an equation for its calculation should be derived. Using Eq. (37), Eq. (39) is reorganized into

$$p_{\text{o,b}} = p_{\text{b}} + \frac{1}{2\rho} \frac{\dot{m}_{\text{b}}^2}{(\mathbf{e_{\text{v}}} \cdot \mathbf{S}_{\text{b}})^2}.$$
 (40)

A relation between mass flow rate, pressure, and their corrections at the boundary element can be developed as

$$\frac{\partial p_{\mathbf{b}}}{\partial \dot{m}_{\mathbf{b}}} \approx \frac{p_{\mathbf{b}} - p_{\mathbf{b}}^*}{\dot{m}_{\mathbf{b}} - \dot{m}_{\mathbf{b}}^*} = \frac{p'_{\mathbf{b}}}{\dot{m}'_{\mathbf{b}}} \Rightarrow p'_{\mathbf{b}} = \frac{\partial p_{\mathbf{b}}}{\partial \dot{m}_{\mathbf{b}}} \dot{m}'_{\mathbf{b}}. \tag{41}$$

Combining Eqs. (41) and (23), a relation between $\dot{m}'_{\rm b}$ and $p'_{\rm C}$ is obtained as

$$\dot{m}_{\rm b}' = \frac{\rho_{\rm b}^* \mathcal{D}_{\rm C}}{1 + \rho_{\rm b}^* \mathcal{D}_{\rm C} \frac{\partial p_{\rm b}}{\partial \dot{m}_{\rm b}}} p_{\rm C}' \tag{42}$$

An expression for $\partial p_b/\partial \dot{m}_b$ is found by differentiating Eq. (40) with respect to \dot{m}_b and is given by

$$\frac{\partial p_{\rm b}}{\partial \dot{m}_{\rm b}} = -\frac{1}{\rho} \frac{\dot{m}_{\rm b}}{\left(\mathbf{e}_{\rm v} \cdot \mathbf{S}_{\rm b}\right)^2} \tag{43}$$

Replacing $\dot{m}'_{\rm b}$ given by Eq. (42) in Eq. (21), the modified $a_{\rm C}^{p'}$ for the boundary element becomes

$$a_{\mathrm{C}}^{p'} = \sum_{f = \text{interior } nb(C)} \rho_{\mathrm{f}} \mathcal{D}_{\mathrm{f}} + \underbrace{\frac{\rho_{\mathrm{b}}^* \mathcal{D}_{\mathrm{C}}}{1 + \rho_{\mathrm{b}}^* \mathcal{D}_{\mathrm{C}} \frac{\hat{o}_{p_{\mathrm{b}}}}{\hat{o}_{m_{\mathrm{b}}}}}}_{\text{boundary face contribution}}$$
(44)

Energy equation

For this boundary condition, the temperature is usually specified. Therefore, the algebraic equation of the boundary element is modified according to Eq. (36).

Physical condition: Outlet

The following outlet boundary conditions are considered (Figure 4): (i) a specified static pressure, (ii) a specified mass flow rate, and (iii) a fully developed flow.

Boundary condition: Specified static pressure

Momentum equation

When the static pressure is known at the outlet (Figure 4a), a fully developed flow is expected and is enforced by setting the component of the gradient of the velocity vector normal to the outlet to zero. The outlet velocity is extrapolated from the value at the boundary element centroid by first equating

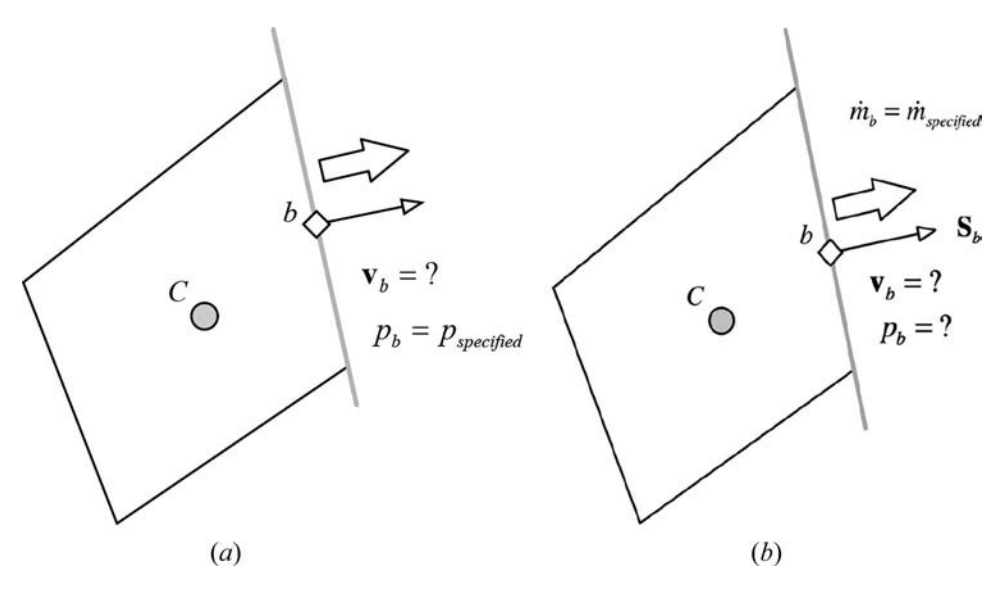


Figure 4. Schematics of (a) specified static pressure, and (b) specified mass flow rate boundary conditions at outlet.

the velocity gradient at the boundary to the normal component at cell centroid (to guarantee that the component normal to the surface is zero) yielding

$$\nabla \mathbf{v}_{b} = \nabla \mathbf{v}_{C} - (\nabla \mathbf{v}_{C} \cdot \mathbf{e}_{b}) \mathbf{e}_{b} \tag{45}$$

and then computing \mathbf{v}_b as

$$\mathbf{v}_{b} = \mathbf{v}_{C} + \nabla \mathbf{v}_{b} \cdot \mathbf{d}_{Cb} \tag{46}$$

With this treatment the modified coefficients become

$$a_{\rm C}^{\bf v} = \underbrace{a_{\rm C}^{\bf v}}_{\text{interior faces contribution}} + \underbrace{\dot{m}_{\rm b}}_{\text{boundary face contribution}}$$

$$a_{F=b}^{\bf v} = 0$$

$$\mathbf{b}_{\rm C}^{\bf v} = \underbrace{\mathbf{b}_{\rm C}^{\bf v}}_{\text{interior faces contribution}} - \underbrace{\dot{m}_{\rm b}(\nabla \mathbf{v}_{\rm b} \cdot \mathbf{d}_{\rm Cb}) - p_{\rm b} \mathbf{S}_{\rm b}}_{\text{boundary face contribution}}$$

$$(47)$$

Pressure correction equation

Since p_b is known, the pressure correction is zero while \dot{m}_b' is not and is calculated from Eq. (23). The direction of \mathbf{v}_b is needed and is usually set equal to \mathbf{v}_C . The $a_C^{p'}$ coefficient in the p' equation is modified as

$$a_{\rm C}^{p'} = \sum_{f = \text{interior } nb(C)} \rho_{\rm f} \mathcal{D}_{\rm f} + \underbrace{\rho_{\rm b} \mathcal{D}_{\rm C}}_{\text{boundary face contribution}}$$
(48)

Energy equation

For the energy equation, the gradient of temperature which is normal to the boundary is set to zero. Thus, the term $(k \nabla T \cdot \mathbf{S})_b$ is zero with the temperature extrapolated from the value at the centroid of the boundary element using Eqs. (45) and (46) with \mathbf{v} replaced by T. The modified coefficients are given by

$$a_{\rm C}^T = \underbrace{a_{\rm C}^T}_{\text{interior faces contribution}} + \underbrace{\dot{m}_{\rm b}c_{\rm p,b}}_{\text{boundary face contribution}}$$

$$a_{F=b}^T = 0$$

$$b_{\rm C}^T = \underbrace{b_{\rm C}^T}_{\text{interior faces contribution}} - \dot{m}_{\rm b}c_{\rm p,b}(\nabla T_{\rm b} \cdot \mathbf{d}_{\rm Cb})$$
interior faces contribution boundary face contribution

Boundary condition: Specified mass flow rate

Momentum equation

A specified uniform mass flow rate (Figure 4b) indicates a known normal velocity component. To be able to calculate \mathbf{v}_b , it is assumed to have the same direction as \mathbf{v}_C , i.e., $(\mathbf{e}_{\mathbf{v}})_b = (\mathbf{e}_{\mathbf{v}})_C$. Thus, $||\mathbf{v}_b||$ is computed as

$$\|\mathbf{v}_{\mathbf{b}}\| = \frac{\dot{m}_{\mathbf{b}}}{\rho_{\mathbf{b}}(\mathbf{e}_{\mathbf{v}})_{C} \cdot \mathbf{S}_{\mathbf{b}}} \tag{50}$$

The known \mathbf{v}_b is used to enforce a specified velocity boundary condition and the coefficients of the algebraic equation of the boundary elements of the momentum equation are modified according to Eq. (35).

Pressure correction equation

Since \dot{m}_b is specified, \dot{m}'_b does not appear in the p' equation. Further, Eq. (23) indicates that $p'_b = p'_C$.

Energy equation

For the energy equation, the gradient of temperature normal to the boundary is set to zero. Thus, the modification to the coefficients of the boundary element follows Eq. (49).

Boundary condition: Fully developed flow

In analyzing fully developed flows, the outlet section should not be located in any recirculation region. Assuming this condition is satisfied, the modifications to the equations are as described below.

Momentum equation

For the momentum equation, the normal velocity gradient is set to zero and \mathbf{v}_b is computed using Eqs. (45) and (46). The boundary pressure is extrapolated from the interior of the domain using

$$p_{\rm b} = p_{\rm C} + \nabla p_{\rm C} \cdot \mathbf{d}_{\rm Cb} \tag{51}$$

Thus the computed \mathbf{v}_b is used to enforce a specified velocity boundary condition and the coefficients of the algebraic equation for the boundary elements are altered according to Eq. (35).

Pressure correction equation

Knowing the velocity \mathbf{v}_b allows computing \dot{m}_b thereby eliminating the need for any mass flow rate correction. Thus \dot{m}_b' is set to zero and dropped from the equation of the boundary elements. Because



 $\mathbf{v}_{\mathbf{h}}$ is not the correct solution at the outlet until convergence is reached, the overall mass conservation is not satisfied. With incompressible flows, overall mass conservation is enforced at any iteration via a special treatment based on modifying m_b . This is achieved by computing the total mass flow rates entering $\sum \dot{m}_{\rm in}$ and leaving $\sum \dot{m}_{\rm out}$ which is the domain and modifying the mass flow rate at an outlet using

$$\dot{m}_{\text{out}} = \dot{m}_{\text{out}} \frac{\sum \dot{m}_{\text{in}}}{\sum \dot{m}_{\text{out}}} \tag{52}$$

Energy equation

Again the gradient of temperature normal to the boundary is set to zero. Thus, the coefficients of the boundary element of the energy equation are modified according to Eq. (49).

Geometric condition: Symmetry

Only one set of equations applies at a symmetry boundary condition. The purpose of its use is to reduce the size of the computational domain and is applicable along a symmetry plane that subdivides the physical domain of interest into two parts that mirrors each other when the solution for all variables is symmetrical. As a symmetry plane reflects scalar variables, a symmetry boundary condition is imposed by setting the fluxes or the normal gradient of all scalar variables to zero. For a vector equation (like momentum), it is a little more complicated. The modifications along a symmetry boundary condition for the momentum, pressure correction, and energy equations of a boundary element are described next.

Momentum equation

Since no flow crosses a symmetry plane (Figure 5), the velocity component normal to the symmetry plane is zero while the component parallel to the symmetry plane retains its magnitude and direction. Mathematically this is written as

$$\mathbf{v}_{\perp} = 0$$

$$\frac{\partial \mathbf{v}_{//}}{\partial n} = 0$$
(53)

where \mathbf{v}_{\perp} and $\mathbf{v}_{\prime\prime}$ are as defined in Eq. (25). Therefore, opposite to a no-slip wall boundary condition, the shear stress is zero while the normal stress is not. Thus, the boundary force is given by

$$\mathbf{F}_{b} = \sigma_{\perp} S_{b} \simeq -2\mu_{b} \frac{(\mathbf{v}_{C})_{\perp}}{d_{\perp}} S_{b} \tag{54}$$

where σ_{\perp} is the normal stress. Since the pressure gradient normal to the symmetry plane is zero, the pressure is computed using Eqs. (45) and (46) with \mathbf{v} replaced by p.

The modifications to the coefficients of the boundary elements for the momentum equation in the x, y and z directions are given in Table 1b (rows 1–3).

Pressure correction equation

Since no flow crosses a symmetry plane, \dot{m}'_b is zero. Thus similar to a wall boundary condition no modification to the coefficients is required as shown in row 4 of Table 1b.

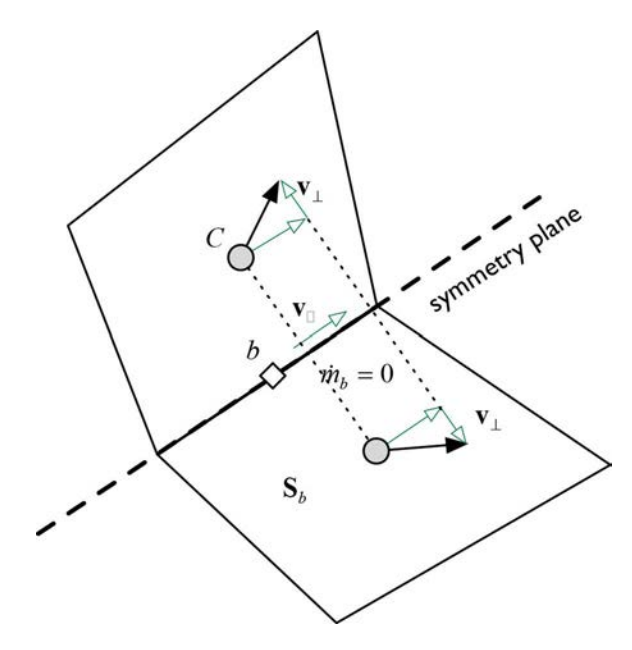


Figure 5. Schematic of a symmetry boundary condition.

Energy equation

Similar to pressure, the gradient of the temperature which is normal to the boundary is set to zero. Thus, the term $(k \nabla T \cdot \mathbf{S})_b$ is zero with the temperature extrapolated from the value at the centroid of the boundary element using Eqs. (45) and (46) with v replaced by T. Since $\dot{m}_{\rm b}$ is zero, the boundary contribution is dropped (row 5 in Table 1b).

Geometric condition: Periodic boundary condition

The periodic boundary condition schematically depicted in Figure 6 is used to reduce the computational domain when solutions are periodic in space and is always defined with a pair of boundary surfaces. The pair of surfaces can be either translated (translational periodicity, Figure 6a) or rotated (rotational periodicity, Figure 6b). For both types, each face in a boundary has a corresponding face and neighbor cell on the other boundary, in accordance with the geometric transformation (i.e., translation or rotation).

With translational periodicity, the same relation governs scalar (pressure, density, etc.) and vector (velocity, gradients) variables. Since in rotational periodicity the coordinate system is rotated, all vector quantities have to be transformed accordingly. On the other hand, scalar quantities remain unchanged.

Table 1b. Modified coefficients of the momentum, continuity, and energy equations for a symmetry boundary condition.

	a_{C}	$a_{F=b}$	b_{C}
	interior faces contribution	=	interior faces contribution
	+		+
1	$\frac{2\mu_{\rm b}S_{\rm b}}{d}e_{\perp x}^2$	0	$-\frac{2\mu_{\rm b}S_{\rm b}}{d}\left[v_{\rm C}e_{\perp v}+w_{\rm C}e_{\perp z}\right]e_{\perp x}-p_{\rm b}S_{\rm b}^{\rm x}$
2	$\frac{a_{\perp}}{d_{\perp}}e_{\perp y}^{2}$	0	$-\frac{2\mu_{b}S_{b}}{2}[u_{c}e_{+y}+w_{c}e_{+z}]e_{+y}-p_{b}S_{b}^{y}$
3	$\frac{a_{\perp}}{2\mu_{\rm b}S_{\rm b}}e_{\perp z}^2$	0	$\begin{aligned} &-\frac{2\mu_{\rm b}S_{\rm b}}{d_{\perp}} \left[v_{\rm C}e_{\perp y} + w_{\rm C}e_{\perp z} \right] e_{\perp x} - p_{\rm b}S_{\rm b}^x \\ &-\frac{2\mu_{\rm b}S_{\rm b}}{d_{\perp}} \left[u_{\rm C}e_{\perp x} + w_{\rm C}e_{\perp z} \right] e_{\perp y} - p_{\rm b}S_{\rm b}^y \\ &-\frac{2\mu_{\rm b}S_{\rm b}}{d_{\perp}} \left[u_{\rm C}e_{\perp x} + v_{\rm C}e_{\perp y} \right] e_{\perp z} - p_{\rm b}S_{\rm b}^z \end{aligned}$
4	0	0	0
5	0	0	0

In terms of implementation, after defining the addressing between faces and cells at both boundary sides, the discretization process treats the boundary faces as internal. Thus, the flux at the boundary face is written in the same way as for an internal face, except that the variable on the other side of the periodic boundary condition should be connected to the first side, through a transformation relation if needed. For a scalar value, the transformation is simply the identity matrix.

Momentum equation

The discretization of the momentum equation on the boundary face follows exactly the discretization at an interior face with Eq. (7) defining the coefficients, where now the neighbor cell is the corresponding cell on the other boundary (Figure 6). Since the momentum equation is a vector equation, the corresponding velocity \mathbf{v}_{F} of the neighbor cell has to be transformed accordingly with a rotation tensor R. In case of translational periodicity (Figure 6a) the transformation matrix is given by

$$\mathbf{R} = \mathbf{I} \tag{55}$$

where I is the 3×3 identity matrix.

For rotational periodicity of angle θ (positive in the clockwise direction, Figure 6b) around an axis of unit vector $\mathbf{a} = (a_1, a_2, a_3)$ (Figure 6b), the rotation tensor is given by [53]

$$\mathbf{R} = \mathbf{I} + \mathbf{W}^{2}(1 - \cos \theta) + \mathbf{W} \sin \theta = \begin{pmatrix} A_{1} & B_{1} & C_{1} \\ A_{2} & B_{2} & C_{2} \\ A_{3} & B_{3} & C_{3} \end{pmatrix}$$
(56)

where W is the skew symmetric tensor associated with the axis of rotation expressed as

$$\mathbf{W} = \begin{pmatrix} 0 & -a_3 & a_2 \\ a_3 & 0 & -a_1 \\ -a_2 & a_1 & 0 \end{pmatrix}$$
 (57)

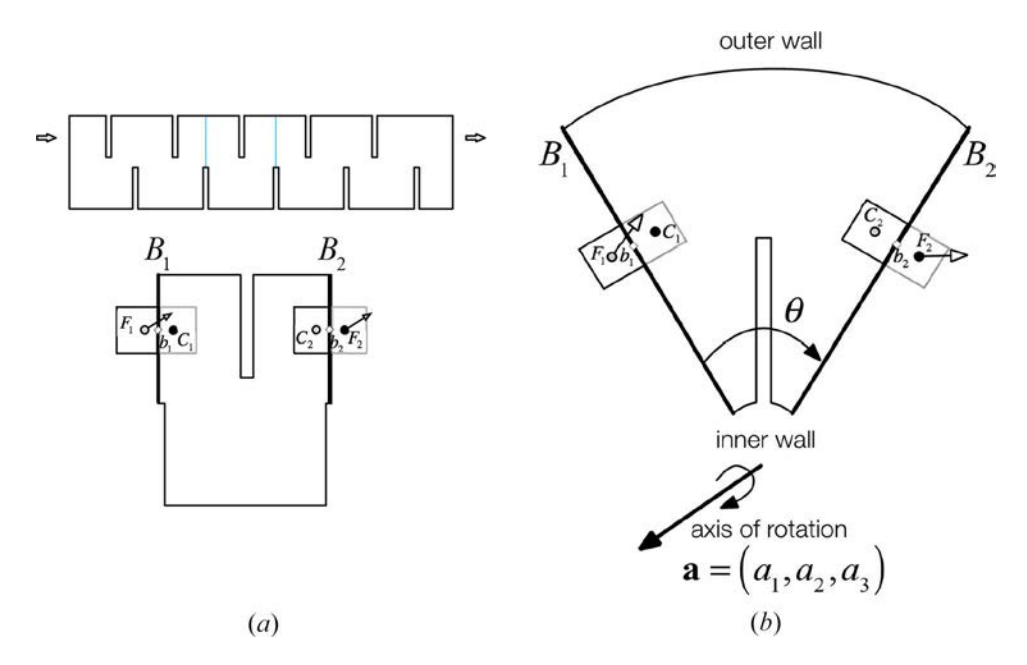


Figure 6. (a) Translational and (b) rotational periodic boundary conditions.

and with the components of R given by

$$A_{1} = 1 - \left(a_{2}^{2} + a_{3}^{2}\right)(1 - \cos\theta) \qquad B_{1} = a_{1}a_{2}(1 - \cos\theta) - a_{3}\sin\theta$$

$$C_{1} = a_{1}a_{3}(1 - \cos\theta) + a_{2}\sin\theta$$

$$A_{2} = a_{1}a_{2}(1 - \cos\theta) + a_{3}\sin\theta \qquad B_{2} = 1 - \left(a_{1}^{2} + a_{3}^{2}\right)(1 - \cos\theta)$$

$$C_{2} = a_{2}a_{3}(1 - \cos\theta) - a_{1}\sin\theta$$

$$A_{3} = a_{1}a_{3}(1 - \cos\theta) - a_{2}\sin\theta \qquad B_{3} = a_{2}a_{3}(1 - \cos\theta) + a_{1}\sin\theta$$

$$C_{3} = 1 - \left(a_{1}^{2} + a_{2}^{2}\right)(1 - \cos\theta)$$

$$(58)$$

Then, the velocity of the neighbor to the element at boundary B_1 (Figure 6a or 6b) is written in terms of the element velocity at boundary B_2 as

$$\mathbf{v}_{F_1} = \mathbf{R}\mathbf{v}_{C_2} = \begin{bmatrix} A_1 u_{C_2} + B_1 v_{C_2} + C_1 w_{C_2} \\ A_2 u_{C_2} + B_2 v_{C_2} + C_2 w_{C_2} \\ A_3 u_{C_2} + B_3 v_{C_2} + C_3 w_{C_2} \end{bmatrix}$$
(59)

Since scalars are invariant with respect to coordinate rotation, the values of pressure, density, and temperature of the neighbor to the element at boundary B_1 are given by

$$p_{F_1} = p_{C_2} \quad \rho_{F_1} = \rho_{C_2} \quad T_{F_1} = T_{C_2} \tag{60}$$

The mass flow rate at the boundary face is computed using the Rhie-Chow interpolation as

$$\dot{m}_{b_1} = \rho_{b_1} \left[\overline{\mathbf{v}_{b_1}} \cdot \mathbf{S}_{b_1} - \overline{\mathcal{D}_{b_1}} (p_{C_2} - p_{C_1}) - \left(\overline{\mathbf{D}_{b_1}^{\mathbf{v}}} \nabla p_{b_1} \cdot \mathbf{T}_{b_1} - \overline{\mathbf{D}_{b_1}^{\mathbf{v}}} \nabla p_{b_1} \cdot \mathbf{S}_{b_1} \right) \right] + \underbrace{\left(\frac{\dot{m}_{b_1}^*}{\rho_{b_1}^*} \right) \rho_{b_1} - \dot{m}_{b_1}^*}_{\text{Compressible}}$$
(61)

where interpolated values are obtained by linear interpolation according to

$$\overline{\square}_{b_1} = \frac{C_2 b_2}{C_1 b_1 + C_2 b_2} \square_{C_1} + \frac{C_1 b_1}{C_1 b_1 + C_2 b_2} \square_{F_1}$$
(62)

With estimates for all variables computed at every iteration, the segregated approach adopts a Dirichlet-like condition in the calculation of the convection, diffusion, and pressure gradient terms leading to the following modified coefficients in the algebraic equation for the boundary element C_1 :

$$\mathbf{b}_{C_1}^{\mathbf{v}} = \mathbf{b}_{C_1}^{\mathbf{v}} - a_{F_1}^{\mathbf{v}} \underbrace{\mathbf{v}_{F_1}}_{=\mathbf{R}\mathbf{v}_{C_2}}$$

$$a_{F_1}^{\mathbf{v}} = 0$$
(63)

Similar modifications are required for element C_2 .

Pressure correction equation

For the mass flow rate across a periodic boundary condition, the corresponding correction \dot{m}'_{b_1} is given by

$$\dot{m}'_{b_1} = -\rho_{b_1}^* \overline{\mathcal{D}_{b_1}} \Big(p'_{C_2} - p'_{C_1} \Big) + \underbrace{\left(\frac{\dot{m}_{b_1}^*}{\rho_{b_1}^*} \right)}_{\text{compressible contribution}} C_{\rho, b_1} p'_{b_1} , \qquad (64)$$



leading to the following modifications to the coefficients of the algebraic equation for the boundary element C_1 :

$$b_{C_{1}}^{p'} = b_{C_{1}}^{p'} - a_{F_{1}}^{p'} \underbrace{p'_{F_{1}}}_{=p'_{C_{2}}}$$

$$a_{F_{1}}^{p'} = 0$$
(65)

The additional source term can be neglected since at convergence the pressure correction field is zero.

Energy equation

Again the treatment for the energy equation only requires that the connection from the periodic cell to its neighbor be done appropriately, leading to the following modified coefficients for the algebraic equation of the boundary element C_1 :

$$b_{C_1}^T = b_{C_1}^T - a_{F_1}^T \underbrace{T_{F_1}}_{=T_{C_2}}$$

$$a_{F_1}^T = 0$$
(66)

Compressible flow

The implementation of boundary conditions in the momentum and energy equations is generally independent of whether the flow is incompressible or compressible. Therefore, the modifications presented for incompressible flow are applicable to compressible flow and will not be repeated. The only difference is with a prescribed stagnation temperature at the inlet instead of static temperature. In this case, the static temperature is extracted based on the known or computed velocity field and the boundary condition is treated like a known static temperature.

As described next, the main difference in the implementation is in the pressure correction equation at inlet and outlet boundaries where an additional convection-like term resulting from density correction appears for compressible flow.

Physical condition: Inlet

The conditions to be imposed at inlet and outlet boundaries depend on whether the flow is subsonic or supersonic as it affects the mathematical type of the equation (i.e., elliptic or hyperbolic).

Subsonic flow

The same boundary conditions discussed for incompressible flow can be imposed for subsonic compressible flow. For transonic flows, it is advisable to specify the stagnation pressure and velocity direction.

Boundary condition: Specified velocity

For compressible flow a specified velocity (Figure 3a) does not imply a known mass flow rate since the density depends on pressure (i.e., $\dot{m}_b' = \rho_b' \mathbf{v}_b^* \cdot \mathbf{S}_b \neq 0$). Moreover, assuming an ideal gas, density correction can be written in terms of p' as

$$\rho' = p'/RT = C_{\rho}p' \tag{67}$$

Therefore, expressing p'_b in terms of internal nodes using a zero order interpolation profile (i.e., $p'_b = p'_c$), the modified coefficient for the boundary element is obtained as

$$a_{\mathrm{C}}^{p'} = \frac{V_{\mathrm{C}}C_{\mathrm{\rho}}}{\Delta t} + \underbrace{\sum_{f=nb(C)} \left(\frac{C_{\mathrm{\rho,f}}}{\rho_{\mathrm{f}}^{*}} \left\| \dot{m}_{\mathrm{f}}^{*}, 0 \right\| \right) + \sum_{f=nb(C)} \rho_{\mathrm{f}}^{*} \mathcal{D}_{\mathrm{f}}}_{\text{interior faces contribution}} + \underbrace{C_{\mathrm{\rho,b}} \frac{\dot{m}_{\mathrm{b}}^{*}}{\rho_{\mathrm{b}}^{*}}}_{\text{boundary face contribution}}$$
(68)

Boundary condition: Specified static pressure and velocity direction

For a specified static pressure at the inlet (Figure 3b), the pressure correction is zero and based on Eq. (67) the density correction is also zero. Thus, the implementation of this boundary condition follows that for incompressible flow presented earlier, with the modified coefficient for the boundary element computed as

$$a_{\mathrm{C}}^{p'} = \frac{V_{\mathrm{C}}C_{\mathrm{p}}}{\Delta t} + \underbrace{\sum_{f=nb(C)} \left(\frac{C_{\mathrm{p,f}}}{\rho_{\mathrm{f}}^{*}} \left\| \dot{m}_{\mathrm{f}}^{*}, 0 \right\| \right) + \sum_{f=nb(C)} \rho_{\mathrm{f}}^{*} \mathcal{D}_{\mathrm{f}}}_{\text{boundary face contribution}} + \underbrace{\sum_{f=nb(C)} \rho_{\mathrm{b}}^{*} \mathcal{D}_{\mathrm{C}}}_{\text{boundary face contribution}}$$
(69)

Boundary condition: Specified total pressure and velocity direction

The procedure followed for the implementation of this boundary condition, shown schematically in Figure 3c, is slightly different than the one used with incompressible flow. The main difference is in the use of the volume flow rate, rather than the mass flow rate, for the calculation of the velocity correction at the inlet boundary. In [44], the mass flow rate was used in the derivations. However, for problems with large drop in density at the inlet the new formulation presented below resulted in better convergence behavior. The use of the new procedure with incompressible flow leads to the same results reported above since the density is constant.

For compressible flow, the total pressure relation is given by

$$p_{\text{o,b}} = p_{\text{b}} \left(1 + \frac{\gamma - 1}{2} M_{\text{b}}^2 \right)^{\gamma / (\gamma - 1)} \tag{70}$$

where γ refers to the ratio of specific heats, and M_b to the Mach number at inlet.

The velocity flux at the boundary is expressed using the Rhie-Chow interpolation as

$$U_{b} = \mathbf{v}_{b} \cdot \mathbf{S}_{b} = \mathbf{v}_{C} \cdot \mathbf{S}_{b} - \mathcal{D}_{C}(p_{b} - p_{C}) - \left(\mathbf{D}_{C} \nabla p_{b}^{*} \cdot \mathbf{T}_{b} - \mathbf{D}_{C} \nabla p_{C}^{*} \cdot \mathbf{S}_{b}\right)$$
(71)

with its correction given by

$$U_{\rm b}' = -\mathcal{D}_{\rm C} \left(p_{\rm b}' - p_{\rm C}' \right) \tag{72}$$

Moreover, a Taylor series expansion leads to

$$p_{\rm b}' = \frac{\partial p_{\rm b}}{\partial U_{\rm b}} U_{\rm b}'. \tag{73}$$

Combining Eq. (72) with Eq. (73), the pressure correction at the boundary is given by

$$p_{\rm b}' = \frac{\frac{\hat{c}p_{\rm b}}{\hat{c}U_{\rm b}}\mathcal{D}_{\rm C}}{1 + \frac{\hat{c}p_{\rm b}}{\hat{c}U_{\rm b}}\mathcal{D}_{\rm C}}p_{\rm C}' = c_1 p_{\rm C}' \tag{74}$$

The velocity vector at the boundary can be expressed in terms of U_b as

$$\mathbf{v}_{b} = \frac{U_{b}}{\mathbf{e}_{\mathbf{v}} \cdot \mathbf{S}_{b}} \mathbf{e}_{\mathbf{v}} \tag{75}$$

while the stagnation pressure becomes

$$p_{0,b} = p_b \left(1 + \frac{(\gamma - 1)}{2\gamma} C_{\rho,b} \left(\frac{U_b}{\mathbf{e_v} \cdot \mathbf{S_b}} \right)^2 \right)^{\gamma/(\gamma - 1)}, \tag{76}$$

leading to the following expression for $\frac{\partial p_b}{\partial U_b}$:

$$\frac{\partial p_b}{\partial U_b} = -\frac{p_b U_b}{T_0 R}. (77)$$

The mass flow rate correction at the boundary becomes

$$\dot{m}_{b}' = \left(\rho_{b}^{*} \mathcal{D}_{C}(1 - c_{1}) + \frac{\dot{m}_{b}^{*}}{\rho_{b}^{*}} C_{\rho, b} c_{1}\right) p_{C}'. \tag{78}$$

Substitution in the pressure correction equation yields the modified coefficient for the boundary element as

$$a_{\mathrm{C}}^{p'} = \frac{V_{\mathrm{C}}C_{\mathrm{p}}}{\Delta t} + \sum_{\underline{f} = nb(C)} \left(\frac{C_{\mathrm{p,f}}}{\rho_{\mathrm{f}}^*} \left\| \dot{m}_{\mathrm{f}}^*, 0 \right\| \right) + \sum_{\underline{f} = nb(C)} \rho_{\mathrm{f}}^* \mathcal{D}_{\mathrm{f}} + \underbrace{\rho_{\mathrm{b}}^* \mathcal{D}_{\mathrm{C}} (1 - c_1) + \frac{\dot{m}_{\mathrm{b}}^*}{\rho_{\mathrm{b}}^*} C_{\mathrm{p,b}} c_1}_{\text{boundary face contribution}}$$
(79)

Supersonic flow

Boundary condition: Specified pressure, velocity, and temperature

If the flow is supersonic at the inlet, then the values for all variables have to be specified implying that $\dot{m}_{\rm b}'=p_{\rm b}'=0$. Thus, for a boundary element, the modified coefficient is written as

$$a_{C}^{p'} = \frac{V_{C}C_{\rho}}{\Delta t} + \underbrace{\sum_{f=nb(C)} \left(\frac{C_{\rho,f}}{\rho_{f}^{*}} \| \dot{m}_{f}^{*}, 0 \| \right) + \sum_{f=nb(C)} \rho_{f}^{*} \mathcal{D}_{f}}_{\text{(80)}}$$

Physical condition: Outlet

Subsonic flow

Boundary condition: Specified pressure

Similar to a specified pressure at the inlet, a specified p_b at the outlet (Figure 4a) implies a zero pressure and density corrections. However, the mass flow rate correction is not zero and is obtained from Eq. (23) by setting p'_b to zero leading to the following modified coefficient for the boundary element:

$$a_{\mathrm{C}}^{p'} = \frac{V_{\mathrm{C}}C_{\mathrm{p}}}{\Delta t} + \sum_{\underline{f} = nb(C)} \left(\frac{C_{\mathrm{p,f}}}{\rho_{\mathrm{f}}^*} \left\| \dot{m}_{\mathrm{f}}^*, 0 \right\| \right) + \sum_{\underline{f} = nb(C)} \rho_{\mathrm{f}}^* \mathcal{D}_{\mathrm{f}} + \underbrace{\rho_{\mathrm{b}}^* \mathcal{D}_{\mathrm{C}}}_{\text{boundary face contribution}}$$
(81)

Boundary condition: Specified mass flow rate

For this boundary condition (Figure 4b), \dot{m}'_b is zero and does not appear in the p' equation with the coefficient of the boundary element computed as

$$a_{\mathrm{C}}^{p'} = \frac{V_{\mathrm{C}}C_{\mathrm{p}}}{\Delta t} + \sum_{f=nb(C)} \left(\frac{C_{\mathrm{p,f}}}{\rho_{\mathrm{f}}^*} \left\| \dot{m}_{\mathrm{f}}^*, 0 \right\| \right) + \sum_{f=nb(C)} \rho_{\mathrm{f}}^* \mathcal{D}_{\mathrm{f}}$$

$$(82)$$

An expression for p_b is obtained from Eq. (23) by setting \dot{m}'_b to zero and is given by

$$p_{b}' = \frac{\rho_{b}^{*} \mathcal{D}_{C}}{\rho_{b}^{*} \mathcal{D}_{C} - \left(\frac{\dot{m}_{b}^{*}}{\rho_{b}^{*}}\right) C_{\rho, b}} p_{C}'$$
(83)

Equation (83) allows computing the boundary pressure and density.

Supersonic flow

Boundary condition: Zero normal gradient

Nothing is specified at a supersonic outlet and all variables are extrapolated from the domain interior. Assuming a zero-order interpolation profile for pressure correction leads to the following modified $a_{\rm C}$ coefficient:

$$a_{\mathrm{C}}^{p'} = \frac{V_{\mathrm{C}}C_{\mathrm{\rho}}}{\Delta t} + \underbrace{\sum_{f=nb(C)} \left(\frac{C_{\mathrm{\rho,f}}}{\rho_{\mathrm{f}}^{*}} \left\| \dot{m}_{\mathrm{f}}^{*}, 0 \right\| \right) + \sum_{f=nb(C)} \rho_{\mathrm{f}}^{*} \mathcal{D}_{\mathrm{f}}}_{\text{interior faces contribution}} + \underbrace{\left(\frac{\dot{m}_{\mathrm{b}}^{*}}{\rho_{\mathrm{b}}^{*}}\right) C_{\mathrm{\rho,b}}}_{\text{boundary face contribution}}$$
(84)

Results and discussion

The boundary conditions described above are realized in a homemade program developed within OpenFOAM* [54], which is a finite volume based open source code framework that can be used to build a variety of CFD solvers based on the finite volume discretization. The solver implements the pressure correction SIMPLE algorithm for both incompressible and compressible flows. Second order schemes are used for convection discretization while Gauss reconstruction and linear interpolation are adopted for second order terms. The chosen test cases validate the previously reported boundary conditions for both incompressible and compressible flows.

Flow around a stator blade

The first validation application focuses on a compressible benchmark test problem based on the work of Goldman et al. [55]. It is a two-dimensional RANS turbulent simulation of a stator blade at midspan. The Reynolds number, based on the chord length and the free-stream velocity, is $Re = 5 \times 10^5$ and the free-stream Mach number is $M_{\infty} = 0.2$. As shown in Figure 7a, total-to-static, symmetry, and periodic boundary conditions are used to reproduce the experimental conditions in a reduced computational domain. The mesh shown in Figure 7b is hybrid of hexahedra in the proximity of the blade and prisms in the outer region, with a total number of 7,200 cells and an average y^+ of 200.

A comparison of predicted blade loading (defined as the ratio of static pressure to the inlet total pressure) with experimental data is shown in Figure 7c. Numerical results are in good agreement with measurements demonstrating the reliability of the presented analysis of boundary conditions.

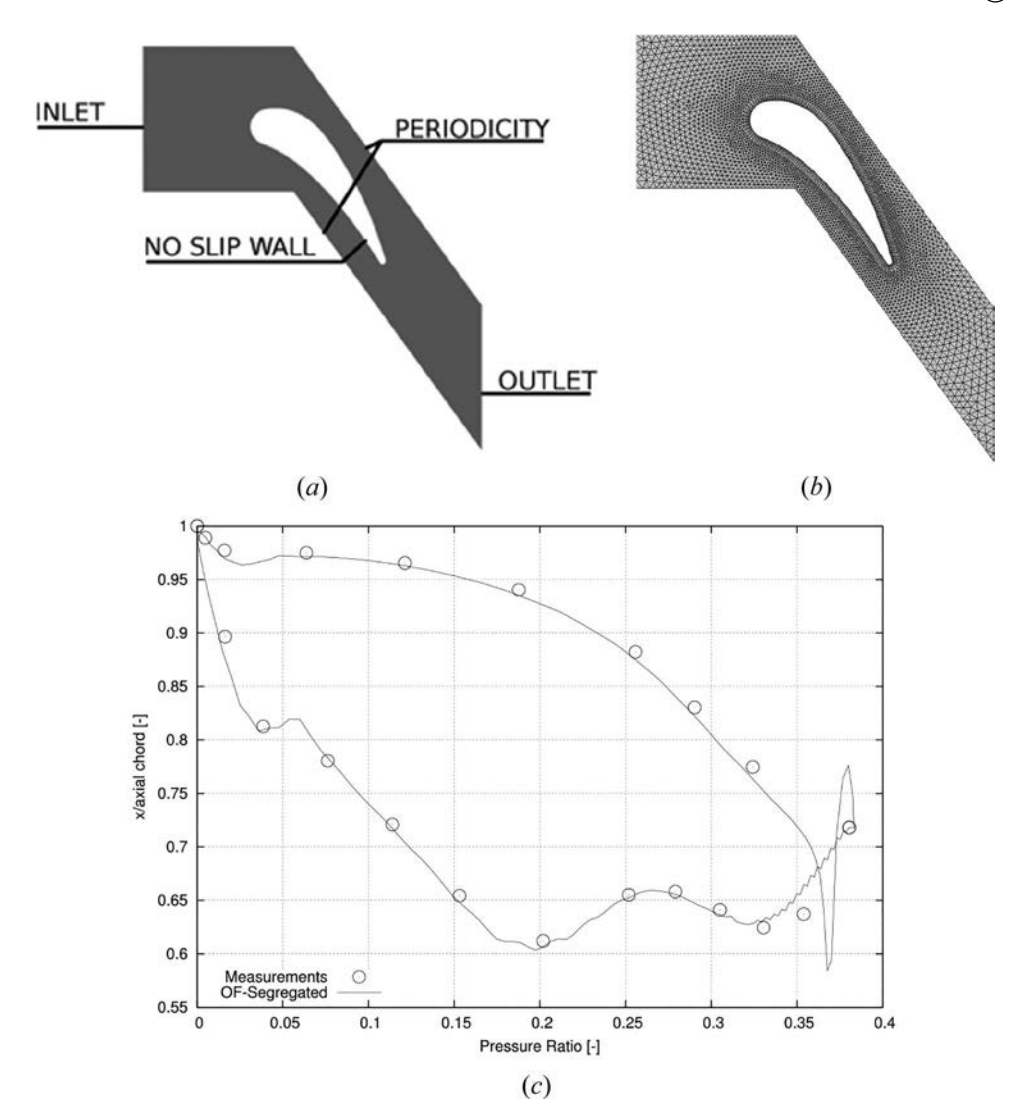


Figure 7. (a) Physical situation and boundary conditions, (b) grid system used, and (c) a comparison of predicted blade loading with the experimental data for the turbulent compressible flow around a stator blade.

The GAMM test

The correct treatment of boundary conditions is again demonstrated by computing the inviscid flow in a channel with either one (Figure 8a) or two (Figure 8b) circular arc airfoils along its centerline, which is denoted in the literature by the GAMM test. Many researchers [19, 48] have used this problem as a benchmark to test their numerical algorithms. Applications of the method to two different inviscid flow types, transonic and supersonic, are presented. The physical configuration for transonic calculations is shown in Figure 8a and it represents a channel of width twice the length of the bump chord ℓ , and of length 3ℓ . For the supersonic case shown in Figure 8b, the same channel width as for the transonic case is used. The total length of the channel is 4.5 ℓ with two bumps, each of chord ℓ , placed in series separated by a distance of 0.5 ℓ . In both cases, the circular arc bumps are placed at a distance ℓ from the channel inlet and outlet. For transonic calculations, the thickness-to-chord ratio is 10% while for supersonic flow calculations it is 4%. The geometric

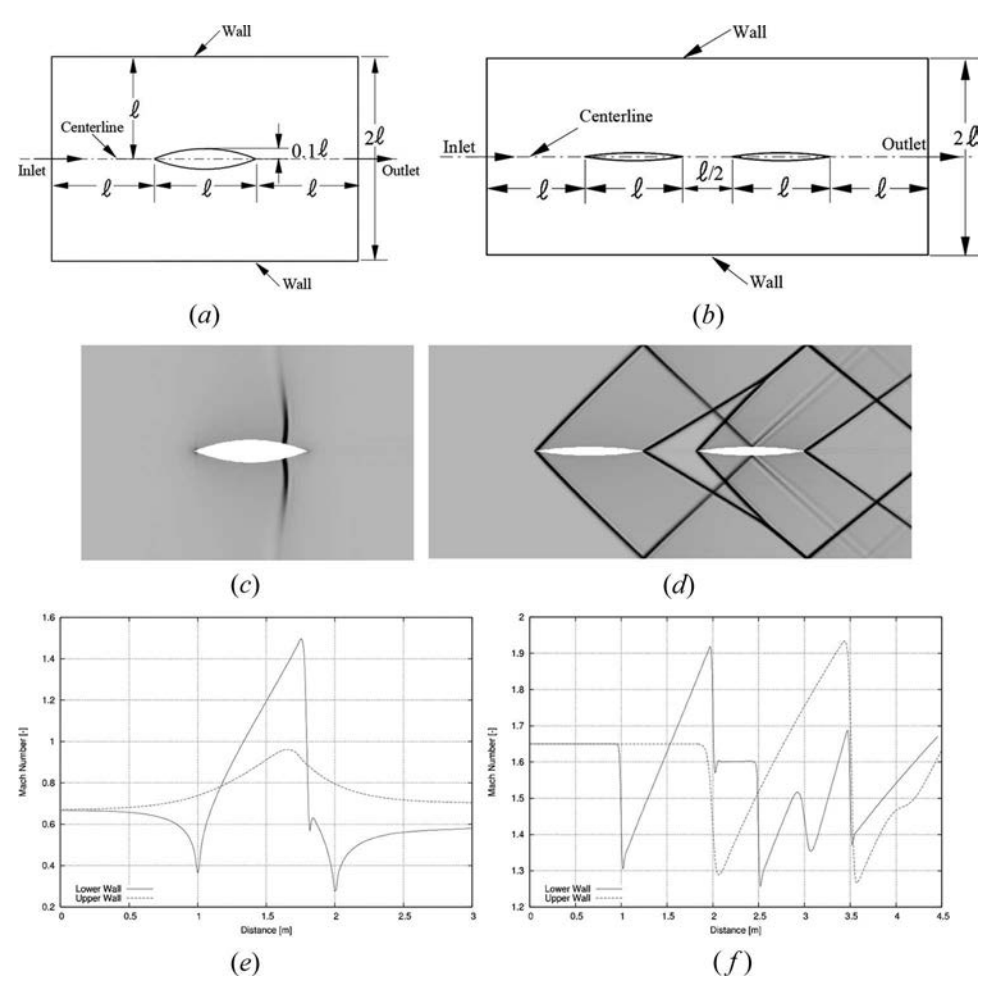


Figure 8. Physical domain (a) for transonic and (b) supersonic flows; Magnitude of density gradient for (c) transonic and (d) supersonic flow; Mach number profiles along the centerline of the domain and the wall of the airfoil (upper part) and the upper wall of the channel in the (e) transonic and (f) supersonic cases.

and flow symmetry are exploited to solve both problems over the upper half of their physical domains. During post processing, solutions are reflected across the horizontal centerline to show fields over the entire domains.

For transonic computations, uniform stagnation conditions are prescribed at the inlet (corresponding to an inlet Mach number of 0.675) along with an axial velocity direction, while at outlet the pressure is assigned. For supersonic flow, all variables are uniformly specified at inlet (resulting in a Mach number with a value of 1.65), while they are extrapolated from the interior solution at the outlet. The slip boundary condition applies at all walls and the symmetry condition along the centerline.

Maps of the density gradient magnitude for both configurations are presented in Figures 8c and d. In addition, the numerically computed Mach number values along the centerline (including the upper wall of the circular arc bumps; designated lower wall in Figures 8e and f) and the outer wall of the channel (designated upper wall in Figures 8e and f) are displayed in Figures 8e and f for the transonic and supersonic cases, respectively. All generated results are in excellent agreement with corresponding ones reported in the literature [19, 48].

Flow around a NACA 0012 airfoil

The last test problem deals with the three-dimensional incompressible flow around a wing with a rounded tip and is based on the work of Dacles-Mariani et al. [56]. Experimentally measured data for the configuration are available for comparison. The physical situation, displayed in Figure 9a, comprises the wing and the wind tunnel. The wing cross-section is a NACA 0012 airfoil with a chord of length 1.22 m. The wing semi-span is 0.91 m. The mesh is in agreement with the restrictions of the low-speed wind tunnel used during measurements. Figure 9b depicts the three-dimensional grid used, which is composed of 1,551,560 elements. As shown, the computational domain extends beyond the physical domain to promote numerical stability. Further, computations are performed over half the width (i.e., half the span of the wing) of the physical domain with the symmetry plane located at the middle of the wing.

As for boundary conditions, a uniform velocity field is specified at the inlet where a turbulence length scale and intensity are prescribed for the turbulence quantities. A uniform pressure is imposed at the outlet and the symmetry boundary condition is applied along the symmetry plane.

To compare numerical results with experimental data, a cross-flow velocity is defined as

$$U_{\rm crossflow} = \sqrt{v^2 + u^2} / U_{\rm inlet} \tag{85}$$

and predicted and measured profiles of $U_{\rm crossflow}$ at two stream-wise locations are displayed in Figures 9c and d. The first location is in the vertical plane at the trailing edge of the wing, while the second is in the vertical plane located at a distance 0.24c beyond the wing. At both locations, profiles are along horizontal lines (i.e., in the span wise direction) that pass through the developed wingtip vortex core [56]. Numerical results are in good agreement with measurements demonstrating the correctness of the presented analysis of boundary conditions.

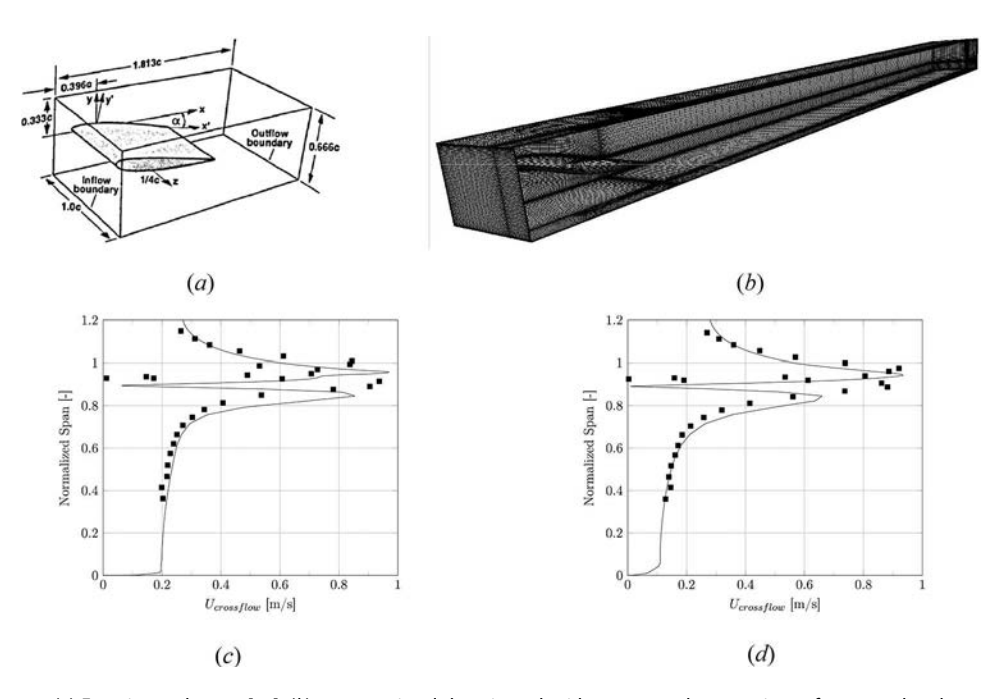


Figure 9. (a) Experimental setup [41]; (b) computational domain and grid system used; comparison of measured and numerically computed $U_{crossflow}$ profiles along the horizontal line passing through the vortex core at the following two positions in the streamwise direction: (c) airfoil trailing edge, and (d) 0.24c beyond the trailing edge.



Closing remarks

The paper described the formulation of boundary conditions encountered in solving incompressible and compressible flow problems. Issues related to the implementation of boundary conditions in the context of a segregated pressure-based unstructured FVM were thoroughly clarified. Specifically, the modifications to the coefficients of the algebraic equations at boundary elements were detailed. Several incompressible and compressible flow problems involving many of the presented boundary conditions were solved and their solutions are shown to be in agreement with published experimental and/or numerical data, confirming correctness of the suggested formulation.

References

- [1] S. V. Patankar, A Calculation Procedure for Two Dimensional Elliptic Situations, Numer. Heat Transfer, vol. 4, no. 4, pp. 409-425, 1981.
- [2] S. V. Patankar, Numerical Heat Transfer and Fluid Flow, Hemisphere, New York, 1981.
- [3] S. V. Patankar, and D. B. Spalding, A Calculation Procedure for Heat, Mass and Momentum Transfer in Three-Dimensional Parabolic Flows, Int. J. Heat Mass Transf., vol. 15, pp. 1787-1806, 1972.
- [4] J. P. Van Doormaal and G. D. Raithby, Enhancement of the SIMPLE Method for Predicting Incompressible Fluid Flows, Numer. Heat Transfer, vol. 7, pp. 147-163, 1984.
- [5] D. B. Spalding, Mathematical Modelling of Fluid Mechanics, Heat Transfer and Mass Transfer Processes, Mechanical Engineering Department, Report HTS/80/1, Imperial College of Science, Technology, and Medecine, London, 1980.
- [6] J. P. Van Doormaal and G. D. Raithby, An Evaluation of the Segregated Approach for Predicting Incompressible Fluid Flows, ASME Paper 85-HT-9, Presented at the National Heat Transfer Conference, Denver, Colorado, August 4-7, 1985.
- [7] S. Acharya and F. Moukalled, Improvements to Incompressible Flow Calculation on a Non-Staggered Curvilinear Grid, Numer. Heat Transfer Part B Fundam., vol. 15, pp. 131-152, 1989.
- [8] R. I. Issa, Solution of the Implicit Discretized Fluid Flow Equations by Operator Splitting, Mechanical Engineering Department, Report FS/82/15, Imperial College, London, 1982.
- [9] C. R. Maliska and G. D. Raithby, Calculating 3-D fluid Flows Using non-orthogonal Grid, Proceedings of the Third International Conference on Numerical Methods in Laminar and Turbulent Flows, Seattle, pp. 656-666,
- [10] R. H. Yen and C. H. Liu, Enhancement of the SIMPLE Algorithm by an Additional Explicit Corrector Step, Numer. Heat Transfer Part BFundam., vol. 24, pp. 127-141, 1993.
- [11] T. Gjesdal and M. E. H Lossius, Comparison of Pressure Correction Smoothers for Multigrid Solution of Incompressible Flow, Int. J. Numer. Methods Fluids, vol. 25, pp. 393-405, 1997.
- [12] F. Moukalled and M. Darwish, A Unified Formulation of the Segregated Class of Algorithms for Fluid Flow at All Speeds, Numer. Heat Transfer Part B Fundam., vol. 37, no. 1, pp. 103-139, 2000.
- [13] M. Darwish, D. Asmar, and F. Moukalled, A Comparative Assessment within a Multigrid Environment of Segregated Pressure-Based Algorithms for Fluid Flow at all Speeds, Numer. Heat Transfer Part B Fundam., vol. 45, pp. 49-74, 2004.
- [14] H. Ebrahimi-Kebria, M. Darbandi, and S. F. Hosseinizadeh, Numerical Simulation of Low-Mach-number Laminar Mixing and Reacting Flows using a Dual-purpose Pressure-based Algorithm, Numer. Heat Transfer Part B Fundam., vol. 56, no. 9, pp. 495-514, 2011.
- [15] N. Kumar, S. Singh, and J. B. Doshi, Pressure Correction-based Iterative Scheme for Navier-Stokes Equations Using Nodal Integral Method, Numer. Heat Transfer Part B Fundam., vol. 62, no. 4, pp. 264-288, 2012.
- [16] S. Vakilipour and S. J. Ormiston, A Coupled Pressure-based Co-located Finite-volume Solution Method for Natural-convection Flows, Numer. Heat Transfer Part B Fundam., vol. 61, no. 2, pp. 91-115, 2012.
- [17] P. Ding and D. L. Sun, A Pressure-based Segregated Solver for Incompressible Flow on Unstructured Grids, Numer. Heat Transfer Part B Fundam., vol. 64, no. 6, pp. 460-479, 2013.
- [18] A. Ashrafizadeh, B. Alinia, and P. Mayeli, A New Co-located Pressure-Based Discretization Method for the Numerical Solution of Incompressible Navier-Stokes Equations, Numer. Heat Transfer Part B Fundam., vol. 67, no. 6, pp. 563-589, 2015.
- [19] K. C. Karki, A Calculation Procedure for Viscous Flows at All Speeds in Complex Geometries, Ph.D. Thesis, University of Minnesota, June 1986.
- [20] W. Shyy and M. E. Braaten, Adaptive Grid Computation for Inviscid Compressible Flows Using a Pressure Correction Method, AIAA Paper 88-3566-CP, 1988.
- [21] C. M. Rhie, A Pressure Based Navier-Stokes Solver Using the Multigrid Method, AIAA Paper 86-0207, 1986.



- [22] F. S. Lien, and M. A. Leschziner, A General Non-Orthogonal Collocated Finite Volume Algorithm for Turbulent Flow at All Speeds Incorporating Second-Moment Trubulence-Transport Closure, Part 1: Computational Implementation, Comput. Methods Appl. Mechan. Eng., vol. 114, pp. 123-148, 1994.
- [23] E. S. Politis and K. C. Giannakoglou, A Pressure-Based Algorithm for High-Speed Turbomachinery Flows, Int. J. Numer. Methods Fluids, vol. 25, pp. 63-80, 1997.
- [24] F. Moukalled and M. Darwish, A High-Resolution Pressure-Based Algorithm for Fluid Flow at All Speeds, J. Comput. Phys., vol. 168, no.1, pp. 101–133, 2001.
- [25] F. Moukalled, A. Doughan, and S. Acharya, Mixed-Convection Heat Transfer in Concave and Convex Channels, AIAA J. Thermophys. Heat Transfer, vol. 13, no. 4, pp. 508-516, 1999.
- [26] F. Moukalled and S. Acharya, Natural Convection in Trapezoidal Cavities with Baffles Mounted on The Upper Inclined Surfaces, Numer. Heat Transfer Part A Appl., vol. 37, no. 6, pp. 545-565, 2000.
- [27] F. Moukalled and S. Acharya, Natural Convection in Trapezoidal Cavities with Two offset Baffles, AIAA J. Thermophys. Heat Transfer, vol. 15, no. 2, pp. 212–218, 2001.
- [28] F. Moukalled and M. Darwish, Natural Convection Heat Transfer in a Porous Rhombic Annulus, Numer. Heat Transfer Part A Appl., vol. 58, no.2, pp. 101-124, 2010.
- [29] F. Moukalled and M. Darwish, Numerical Prediction of Dispersion and Evaporation of Liquid Sprays in Gases Flowing at all Speed, Numer. Heat Transfer Part B Fundam., vol. 54, no. 3, pp. 185-212, 2008.
- [30] F. Moukalled, and M. Darwish, Mixing and Evaporation of Liquid Droplets Injected into an Air Stream Flowing at all Speed, Phys. Fluids, vol. 20, no. 4, art. no. 040804, 2008.
- [31] I. Fayssal and F. Moukalled, A New Numerical Approach for Predicting the Two-Phase Flow of Refrigerants During Evaporation and Condensation, Numer. Heat Transfer Part B Fundam., vol. 62, no. 5, pp. 341-369,
- [32] T. Dbouk, E. Lemaire, L. Lobry, and F. Moukalled, Shear-induced Particles Migration: Predictions from Experimental Evaluation of the Particle Stress Tensor, J. Non Newton. Fluid Mechan., vol. 198, pp. 78-95, 2013.
- [33] D. Merhi, E. Lemaire, G. Bossis, and F. Moukalled, Particle Migration in a Concentrated Suspension Flowing between Rotating Parallel Plates: Investigation of Diffusion Flux Coefficients, J. Rheol., vol. 49, no. 6, pp. 1429-1448, 2005.
- [34] Z. Wang, J. Gong, and C. Wu, Numerical Simulation of One-dimensional Two-phase Flow Using a Pressure-based Algorithm, Numer. Heat Transfer Part A Appl., vol. 68, no. 4, pp. 369-387, 2015.
- [35] M. Darwish, A. Abdel Aziz, and F. Moukalled, A Coupled Pressure-based Finite-volume Solver for Incompressible Two-phase Flow, Numer. Heat Transfer Part B Fundam., vol. 67, no. 1, pp. 47-74, 2015.
- [36] F. Moukalled, S. Verma, and M. Darwish, The Use of CFD for Predicting and Optimizing the Performance of Air Conditioning Equipment, Int. J. Heat Mass Transfer, vol. 54, pp. 549–563, 2011.
- [37] C. M. Rhie and W. Chow, A Numerical Study of Turbulent Flow Past an Isolated Airfoil with Trailing Edge Separation, AIAA J., vol. 21, no. 11, pp. 1525–1532,1983.
- [38] L. Mangani, E. Casartelli, and S. Mauri, Assessment of Various Turbulence Models in a High Pressure Ratio Centrifugal Compressor with an Object Oriented CFD Code, J. Turbomach., vol. 134, no. 6, pp. 061033-061033-10, 2012.
- [39] L. Mangani, E. Groschel, B. Rembold, and E. Casartelli, An Object-Oriented CFD Code for Optimization of High Pressure Ratio Compressors, ASME Turbo Expo, Paper no. GT2012-68708, 2012.
- [40] E. Di Carmine, B. Facchini, and L. Mangani, Investigation of Innovative Trailing Edge Cooling Configurations with Enlarged Pedestals and Square or Semicircular Ribs: Part II- Numerical Results, ASME Turbo Expo 2008: Power for Land, Sea, and Air, pp. 943-953, 2008.
- [41] T. S. Park and S.-K. Kim, A Pressure-based Algorithm for Gaseous Hydrogen/Liquid Oxygen Jet Flame at Supercritical Pressure, Numer. Heat Transfer Part A Appl., vol. 67, no. 5, pp. 547-570, 2015.
- [42] F. Moukalled and M. Darwish, Transient Schemes for Capturing Interfaces of Free-Surface Flows, Numer. Heat Transfer Part B Fundam., vol. 61, no. 3, pp. 171-203, 2012.
- [43] M. Darwish and F. Moukalled, Convective Schemes for Capturing Interfaces of Free-Surface Flows on Unstructured Grids, Numer. Heat Transfer Part B Fundam., vol. 49, pp. 19-42, 2006.
- [44] F. Moukalled, L. Managani, and M. Darwish, The Finite Volume Method in Computational Fluid Dyanamics: An Advanced Introduction with OpenFOAM® and Matalab®, Springer, Switzerland, 2015.
- [45] N. Balakrishnan and G. Fernandez, Wall Boundary Conditions for Inviscid Compressible Flows on Unstructured Meshes, Int. J. Numer. Methods Fluids, vol. 28, pp. 1481-1501, 1998.
- [46] L. Gong, Z.-Y. Li, Y.-L. He, and W.-Q. Tao, Discussion on Numerical Treatment of Periodic Boundary Condition for Temperature, Numer. Heat Transfer Part B Fundam., vol. 52, pp. 429-448, 2007.
- [47] S. R. Mathur and J. Y. Murthy, Pressure Boundary Conditions for Incompressible Flow Using Unstructured Meshes, Numer. Heat Transfer Part B Fundam., vol. 32, pp. 283-298, 1997.
- [48] I. Demirdzic, Z. Lilek, and M. Peric, A Collocated Finite Volume Method for Predicting Flows at all Speeds, Int. J. Numer. Methods Fluids, vol. 16, pp. 1029-1050, 1993.
- [49] J. H. Ferziger and M. Peric, Computational Methods for Fluid Dynamics, 3rd ed., Berlin, Springer, 2002.



- [50] I. Demirdzic, Finite-Volume Method for General Geometries Based on Cartesian Velocity Components and Non-staggered Grid Arrangement, Fluids Section Report, Mechanical engineering Department, Imperial College, London, 1983.
- [51] S. Muzaferija and A. D. Gosman, Finite Volume CFD Procedure and Adaptive Error Control Strategy for Grids of Arbitrary Topology, J. Comput. Phys., vol. 138, pp. 766-787, 1997.
- [52] I. Demirdzic, and S. Muzaferija, Numerical Method for Coupled Fluid Flow, Heat Transfer and Stress Analysis Using Unstructured Moving Meshes with Cells of Arbitrary Topology, Comput. Methods Appl. Mechan. Eng., vol. 125, pp. 235-255, 1995.
- [53] O. Rodrigues, Des lois géometriques qui regissent les déplacements d' un systéme solide dans l' espace, et de la variation des coordonnées provenant de ces déplacement considérées indépendent des causes qui peuvent les produire, J. Math. Pures Appl., vol.5, pp. 380-440, 1840.
- [54] OpenFOAM, 2015 Version 2.3.x. http://www.openfoam.org
- [55] L. G. Goldman and K. L. McLallin, Cold-air Annular Cascade Investigation of Aerodynamic Performance of Core-Engine-Cooled Turbine Vanes: I Solid Vane Performance and Facility Description, Technical report, NASA Technical Memorandum, 1977.
- [56] J. Dacles-Mariani, G. Zilliac, S. Chow, P. Bradshaw, Numerical/Experimental Study of a Wingtip Vortex in the Near Field, AIAA J., vol. 33, pp. 1561-1568, 1995.